

(12)

COORDINATED SCIENCE LABORATORY

ADA 125871

AN APPLICATION OF
DIGITAL EXTRAPOLATION
IN ARRAY PROCESSING

H. FAN
E. I. EL-MASRY
W. F. JENKINS

DTIC
ELEGTE
MAR 21 1983
S D D

APPROVED FOR PUBLIC RELEASE. DISTRIBUTION UNLIMITED.

DTIC FILE COPY

83 03 21 001

UNCLASSIFIED

SECURITY CLASSIFICATION OF THIS PAGE (When Data Entered)

REPORT DOCUMENTATION PAGE		READ INSTRUCTIONS BEFORE COMPLETING FORM
1. REPORT NUMBER	2. GOVT ACCESSION NO. AD-A125871	3. RECIPIENT'S CATALOG NUMBER
4. TITLE (and Subtitle) AN APPLICATION OF DIGITAL EXTRAPOLATION IN ARRAY PROCESSING		5. TYPE OF REPORT & PERIOD COVERED Technical Report
7. AUTHOR(s) H. Fan, E. I. El-Masry and W. K. Jenkins		6. PERFORMING ORG. REPORT NUMBER R-983, UILU ENG 83-2204
9. PERFORMING ORGANIZATION NAME AND ADDRESS Joint Services Electronics Program (JSEP)		8. CONTRACT OR GRANT NUMBER(s) N00014-79-C-0424
11. CONTROLLING OFFICE NAME AND ADDRESS		10. PROGRAM ELEMENT, PROJECT, TASK AREA & WORK UNIT NUMBERS
14. MONITORING AGENCY NAME & ADDRESS (if different from Controlling Office)		12. REPORT DATE January 1983
		13. NUMBER OF PAGES 66
		15. SECURITY CLASS. (of this report) UNCLASSIFIED
		15a. DECLASSIFICATION/DOWNGRADING SCHEDULE
16. DISTRIBUTION STATEMENT (of this Report) Approved for public release; distribution unlimited		
17. DISTRIBUTION STATEMENT (of the abstract entered in Block 20, if different from Report)		
18. SUPPLEMENTARY NOTES		
19. KEY WORDS (Continue on reverse side if necessary and identify by block number) Digital Extrapolation Array Processing Beamforming		
20. ABSTRACT (Continue on reverse side if necessary and identify by block number) More sensors are usually required in order to enhance the resolution of a beamformer and to improve its beam pattern. Due to physical and/or economical constraints this requirement cannot be met. This paper presents the results of an analytical and experimental study of the use of a signal extrapolation method in order to "synthetically" (without adding more physical sensors) enhance the beamformer resolution. A simple model for the extrapolation error has been obtained experimentally. The beam pattern and the resolution of the beamformer		

DD FORM 1 JAN 73 1473

UNCLASSIFIED

UNCLASSIFIED

SECURITY CLASSIFICATION OF THIS PAGE(When Data Entered)

have been extensively improved. Further improvements can be achieved by combining other techniques such as windowing, temporal interpolation, etc. to the spatial extrapolation. Examples using Hamming windows are given.

UNCLASSIFIED

SECURITY CLASSIFICATION OF THIS PAGE(When Data Entered)

Accession For	
NTIS GRA&I	<input checked="" type="checkbox"/>
DTIC TAB	<input type="checkbox"/>
Unannounced	<input type="checkbox"/>
Justification	
By _____	
Distribution/	
Availability Codes	
Dist	Avail and/or Special
A	



AN APPLICATION OF DIGITAL EXTRAPOLATION IN ARRAY PROCESSING

BY

H. FAN, E. I. EL-MASRY AND W. K. JENKINS
Coordinated Science Laboratory
University of Illinois

This work was supported by the Joint Services Electronics Program under Contract
N00014-79-C-0424.

SYMBOLS AND NOTATIONS

s	signal to be detected
S	Fourier transform of s
N	$(2M+1) \times 1$ noise vector (white, Gaussian and uncorrelated between any two elements)
n_i	the i th element of N
r_i	received signal at the i th sensor
g	beam output
σ_x^2	variance of the random quantity x
D	distance between two sensors
θ	incidence angle of the incoming signal wave to the linear array of sensors
a, a_0	$\sin\theta, \sin\theta_0$
c	signal propagation speed in the medium
A^+	generalized inverse of the matrix A
$Y^+ (=A^+Z)$	minimum norm least squares solution of the set of linear equations $AY=Z$
$L (= [l_{ij}])$	$\infty \times \infty$ matrix of the low-pass filter operator with cutoff frequency $f_c T$:

$$l_{ij} = \frac{\sin[2\pi(i-j)f_c T]}{\pi(i-j)}; i, j=0, \pm 1, \pm 2, \dots$$

note that its spectrum is one in the frequency range $(-f_c T, f_c T)$, and zero elsewhere

$P (= \{p_{ij}\})$ $(2M+1) \times$ matrix of the truncation operator:

$$p_{ij} = \begin{cases} 1: i=j, -M \leq i, j \leq M \\ 0: \text{otherwise} \end{cases}$$

Δ sampling interval

w weighting function

TABLE OF CONTENTS

CHAPTER	PAGE
1 INTRODUCTION	1
2 BACKGROUND	3
2.1 Beamforming	3
2.2 Extrapolation	8
3 EXTRAPOLATION BEAMFORMING	12
3.1 Real-Time Implementation	12
3.2 Extrapolation Error	15
3.3 Evaluation Of Performance	38
3.3.1 Beam Pattern	40
3.3.2 Signal-To-Noise Ratio	43
4 EXPERIMENTAL RESULTS	48
4.1 Main Results	48
4.2 Effects Of Parameter Changes	56
5 SUMMARY	63
REFERENCES	65

CHAPTER 1

INTRODUCTION

In the area of signal processing, considerable attention has been devoted to digital array processing in recent years. This attention is due to the increasingly wide use of array processing for both civilian and military purposes. Digital beamforming, for example, is popular because of its advantages in speed, accuracy, etc., over conventional analog beamforming. Many papers concerning digital beamforming have recently been published [1]-[8]. It has been shown [1], [8] that the quality of performance of a beamformer, such as beam pattern, signal-to-noise ratio, etc., depends to a great extent on the number of sensors used, i.e., the more sensors used, the better the beam pattern becomes. In a practical situation, however, the number of sensors may be restricted by economical reasons or physical restrictions. In this situation one may weight the output of each sensor before beamforming. This helps to some extent, although the improvement is rather limited.

A totally different issue, signal extrapolation, has also been drawing a great amount of interest recently, largely in the area of spectral estimation. It has been shown that a known portion of a signal can be extrapolated outside of the observation interval if the signal possesses certain property [9], [12]. Many algorithms, both iterative and non-iterative, have been proposed for both continuous and discrete cases. References [9]-[13] serve as a good review on this issue.

The purpose of this thesis is to use spatial signal extrapolation in digital beamforming to improve the beam pattern without adding more physical sensors. Effectively, the sensors are added "synthetically" through signal processing. This has the potential to improve performance considerably. Other currently used techniques such as interpolation, weighting, etc. can be combined with extrapolation to achieve overall better performance.

CHAPTER 2

BACKGROUND

The following discussion assumes a uniform linear array as shown in Fig. 2.1. For convenience, we assume that there is an odd number of sensors in the array. These sensors are indexed from $-M$ to M so that the total number is $2M+1$. Also we assume that the signal is band-limited and the noise is white and Gaussian. Furthermore, we assume that the beam steering specifications are met either by sampling the sensor outputs at a sufficiently high frequency, or by using digital interpolation beamforming techniques, as described in [2]. These assumptions will be used throughout this thesis.

2.1 Beamforming

The task of detecting a signal and determining its direction can be accomplished by digital beamforming, i.e., by delaying and summing the corresponding sensor signals. Suppose the signal is a plane wave which impinges upon the linear array of $2M+1$ sensors at an angle θ_0 with speed c_0 (see Fig. 2.1). The received signal at the i th sensor is denoted by

$$r_i(t) = s\left(t + \frac{id a_0}{c_0}\right) \quad (2.1)$$

where $a_0 = \sin\theta_0$. The beamformer samples the output of each sensor, delays the samples by delay intervals determined by the steering angle, and then sums these delayed samples of the sensor signals along the array

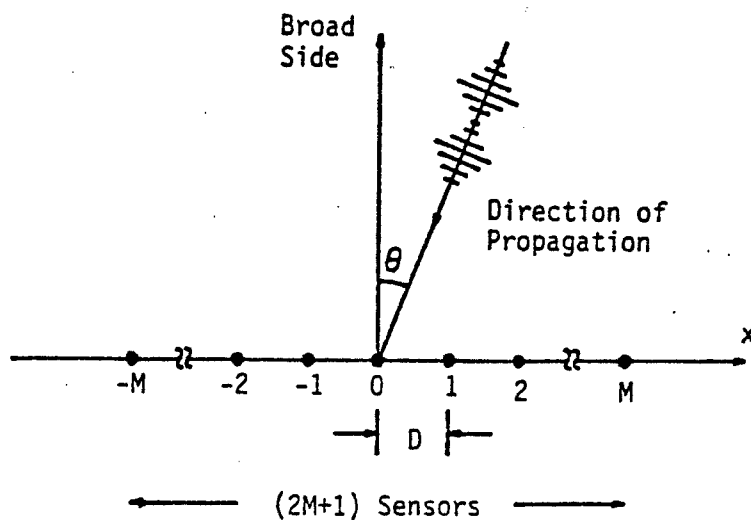


Fig. 2.1 Array geometry

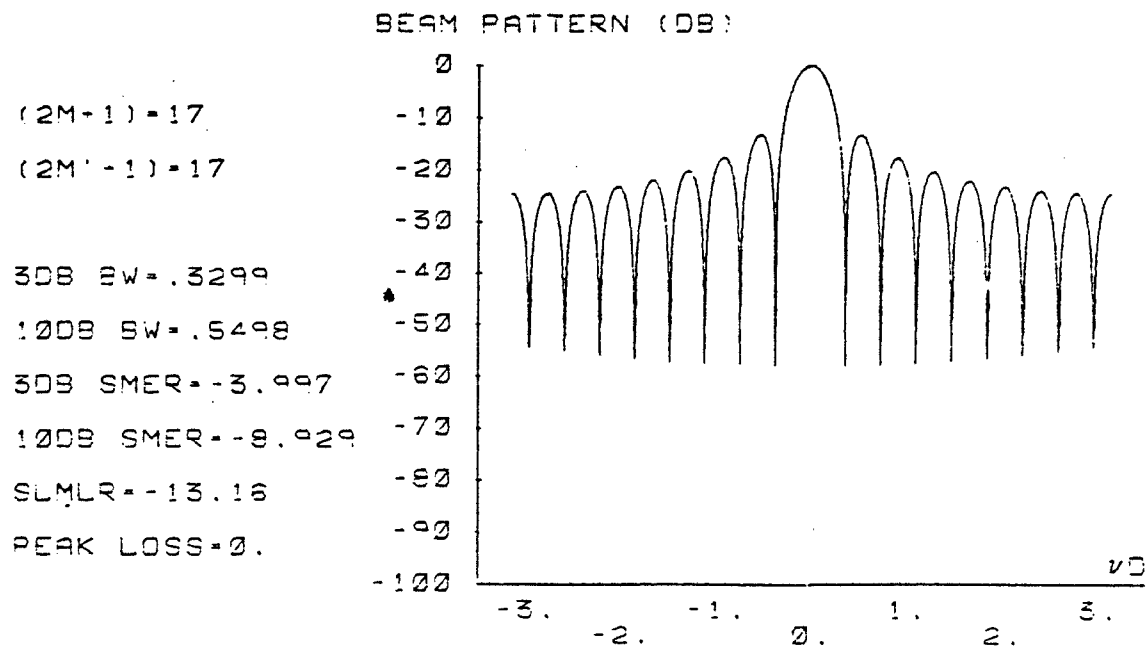


Fig. 2.2 A beam pattern

dimension. This process is described by

$$\begin{aligned}
 g(a, m\Delta) &= \frac{1}{2M+1} \sum_{i=-M}^M r_i(m\Delta - \frac{iDa}{c}) \\
 &= \frac{1}{2M+1} \sum_{i=-M}^M s[m\Delta - iD (\frac{a}{c} - \frac{a_0}{c_0})] \\
 &= \frac{\Delta}{2\pi} \int_{-\pi}^{\pi} S(e^{j\omega m\Delta}) \left[\frac{1}{2M+1} \sum_{i=-M}^M e^{-j\omega iD (\frac{a}{c} - \frac{a_0}{c_0})} \right] e^{j\omega m\Delta} d\omega \\
 &= \frac{\Delta}{2\pi} \int_{-\pi}^{\pi} S(e^{j\omega m\Delta}) W[\omega(\frac{a}{c} - \frac{a_0}{c_0})] e^{j\omega m\Delta} d\omega \quad (2.2)
 \end{aligned}$$

where $S(e^{j\omega m\Delta})$ is the discrete Fourier transform of $s(m\Delta)$, and $W[\omega(\frac{a}{c} - \frac{a_0}{c_0})]$, called the beam pattern, is given by

$$\begin{aligned}
 W(v) &= \frac{1}{2M+1} \sum_{i=-M}^M e^{-jivD} \\
 &= \frac{\sin \frac{(2M+1)}{2} vD}{(2M+1) \sin \frac{vD}{2}} \quad (2.3)
 \end{aligned}$$

The magnitude of a beam pattern is usually displayed on a dB scale as shown in Fig. 2.2 where the horizontal axis is vD . Notice that the beam pattern is periodic with a period of 2π . It is easy to see from Eqn. (2.3) that the largest value occurs at $vD=0$, which coincides with $\frac{a}{c} = \frac{a_0}{c_0}$ when the beam is steered at the angle of the incident signal wave.

The beam output at this angle is $g(a_0, m\Delta) = s(m\Delta)$. Thus the signal and its incidence angle can both be detected. Notice that Da/c must be an integer multiple of Δ because of the sampling, although Da_0/c_0 is continuous. This implies that a digital beamformer cannot steer continuously in the detecting space. However, as we mentioned earlier, it is assumed that the sampling rate is high enough so that all required steering angles are covered.

Also, it is seen that the first zero of $W(\nu)$ occurs when $\nu D = \pm \frac{2\pi}{(2M+1)}$. That is, the main lobe width is inversely proportional to the total number of sensors in the linear array. By increasing the number of sensors, the width of the main lobe of the beam pattern is narrowed, thus improving an important measurement of the beam pattern.

A weighting sequence $w(i)$ can be applied to each sensor output before summation. In this case, Eqn. (2.2) takes the form

$$g(a, m\Delta) = \frac{1}{2M+1} \sum_{i=-M}^M w(i) r_i\left(m\Delta - \frac{iDa}{c}\right), \quad (2.4)$$

and the beam pattern becomes

$$\begin{aligned} W(\nu) &= \frac{1}{2M+1} \sum_{i=-M}^M w(i) e^{-j i \nu D} \\ &= \frac{1}{2M+1} \left[w(0) + 2 \sum_{i=1}^M w(i) \cos i \nu D \right] \end{aligned} \quad (2.5)$$

if $w(i)$ is symmetric. The weights $w(i)$'s are chosen to improve various parameters of the output beam, in much the same way an FIR filter is designed using a window function to shape its spectrum. In general, windowing is a well developed subject in the literature on both filter and antenna design [14], [15].

In the case when there is a noisy background, the signal-to-noise ratio (SNR) at the beam output serves as an essential measurement of performance. Assuming additive white Gaussian noise which is uncorrelated from one sensor to another, the received signal at the i th sensor is

$$r_i(t) = s\left(t + \frac{1Da_0}{c_0}\right) + n_i(t), \quad (2.6)$$

and

$$\begin{aligned} g(a, m\Delta) &= \frac{1}{2M+1} \sum_{i=-M}^M w(i) r_i\left(m\Delta - \frac{1Da}{c}\right) \\ &= \frac{1}{2M+1} \sum_{i=-M}^M w(i) s\left[m\Delta - 1D\left(\frac{a}{c} - \frac{a_0}{c_0}\right)\right] \\ &\quad + \frac{1}{2M+1} \sum_{i=-M}^M w(i) n_i\left(m\Delta - \frac{1Da}{c}\right). \end{aligned} \quad (2.7)$$

At the angle $\frac{\alpha - \alpha_0}{c - c_0}$, the beamformer output becomes

$$g(m\Delta) = \frac{s(m\Delta)}{2M+1} \sum_{i=-M}^M w(i) + \frac{1}{2M+1} \sum_{i=-M}^M w(i) n_i\left(m\Delta - \frac{iDa_0}{c_0}\right). \quad (2.8)$$

The signal-to-noise ratio of $g(m\Delta)$ is defined as

$$\begin{aligned} \text{SNR} &= 10 \log_{10} \left\{ \text{var} \left[\frac{s(m\Delta)}{2M+1} \sum_{i=-M}^M w(i) \right] / \text{var} \left[\frac{1}{2M+1} \sum_{i=-M}^M w(i) n_i\left(m\Delta - \frac{iDa_0}{c_0}\right) \right] \right\} \\ &= 10 \log_{10} \left\{ \sigma_s^2 \left[\frac{1}{2M+1} \sum_{i=-M}^M w(i) \right]^2 / \frac{\sigma_n^2}{(2M+1)^2} \sum_{i=-M}^M w^2(i) \right\} \\ &= 10 \log_{10} \frac{\sigma_s^2}{\sigma_n^2} + 10 \log_{10} \left\{ \left[\sum_{i=-M}^M w(i) \right]^2 / \sum_{i=-M}^M w^2(i) \right\}. \quad (2.9) \end{aligned}$$

The first term in the last expression is the input SNR. The second term is called "array gain". It equals $10 \log_{10}(2M+1)$ when all weights equal one. In other words, beamforming increases SNR by the amount of array gain. Also, note that the array gain increases as the number of sensors increases.

2.2 Extrapolation

The motivation to link digital beamforming and signal extrapolation is quite obvious from the above discussion. Performance of the beam pattern and beam SNR are dependent upon the number of the sensors used.

Often, including a large number of sensors in an array is not practical because of the physical, geometrical, or economical reasons. An excellent approach to solving this problem is well known in the area of SAR (synthetic aperture radar), where a moving sensor (a microwave radar carried on an airplane or a satellite) is used to form a long synthetic array. This approach is not very practical in sonar and underwater sound signal processing for many reasons, such as low propagation speed, low vehicle speed, and instabilities in traveling along a straight path [17]. Thus, it is natural to look for alternate techniques which extend the array beyond its actual physical length.

In 1975, Papoulis [9] proposed an iterative procedure for extrapolating an (continuous) analytic signal based on the observation of only a time limited portion of it. Later, a series of papers concerning this problem was published ([10]-[13], etc.). An important paper discussing discrete extrapolation is due to Jain et al. [12]. For the purpose of this study, only Jain's one step approach will be discussed here.

Let the infinite-dimensional vector $Y = \{y_k: -\infty < k < \infty\}$ denote a sequence, and the $(2M+1) \times 1$ vector Z denote an observation of Y over a limited interval, i.e., $z_j = y_j$ for $-M \leq j \leq M$. Using the truncation operator P , we have

$$Z = PY. \quad (2.10)$$

If y_k 's are the samples of a continuous function $y(t)$ which is band-

limited to the region $(-f_c, f_c)$, then Y is band-limited over $(-f_c T, f_c T)$, where T is the interval between two adjacent samples. Hence, using the low-pass operator L , Y must satisfy $LY=Y$, so that we have

$$Z=PLY=AY \quad (2.11)$$

where $A=PL$. Equation (2.11) is a set of linear equations with infinitely many solutions. However, its minimum norm least squares (MNLS) solution is unique and is given by [12]:

$$Y^+=A^+Z=LP^T\hat{L}^{-1}Z, \quad (2.12)$$

where $\hat{L}=PLP^T$. This is Jain's one-step extrapolation algorithm. Explicitly, we can write

$$Y^+ = H(H1)^{-1}Z \quad (2.13)$$

where H is a $\infty \times (2M+1)$ matrix with each element defined by

$$h_{ij} = \frac{\sin[2\pi(i-j)f_c T]}{\pi(i-j)}; \quad \begin{matrix} i=0, \pm 1, \pm 2, \dots \\ -M \leq j \leq M \end{matrix} \quad (2.14)$$

(Note that the subscripts here are different from the conventional row-column index of a matrix), and $H1$ is a square matrix of dimension $(2M+1)$ with entries given by

$$h1_{ij} = \frac{\sin[2\pi(i-j)f_c T]}{\pi(i-j)}; \quad -M \leq i, j \leq M. \quad (2.15)$$

In case of noisy observation

$$Z = PY + N, \quad (2.16)$$

we have a "mean-square extrapolation":

$$\hat{Y} = H(HI + \gamma I)^{-1} Z \quad (2.17)$$

where $\gamma = \sigma_n^2 / \sigma_y^2$ and I is the identity matrix (also see [12]).

The extrapolated sequence Y^+ (also \hat{Y}) does not equal Y , in general. However, it converges to Y (hence to $y(t)$) when the interval T approaches zero (One more condition is needed for this conclusion, i.e., $y(t)$ has finite energy, see [13]).

CHAPTER 3

EXTRAPOLATION BEAMFORMING

3.1 Real-Time Implementation

Jain's one-step extrapolation procedure can be used for spatial extrapolation, as well as time extrapolation. Specifically, suppose the x -axis describes spatial position along the linear array, and a plane wave $s(t+x\frac{a_0}{c_0})$ impinges upon this array with an incidence angle θ_0 and speed c_0 , as previously shown in Fig. 2.1. The received signal at the i th sensor is $s(t+iD\frac{a_0}{c_0})$ as in Eqn. (2.1). Let the signal $s(t)$ be band-limited over $(-f_c, f_c)$. Hence if $S(f)$ is the continuous Fourier transform of $s(t)$, then $S(f)=0$ for $|f|>f_c$. For a fixed t , the traveling wave $s(t+x\frac{a_0}{c_0})$ is a function of x . Without loss of generality, we may as well assume that $t=0$. Then we define

$$u(x) = s(\frac{a_0}{c_0}x). \quad (3.1)$$

Its Fourier transform is given by

$$U(k) = \frac{c_0}{a_0} S(\frac{c_0}{a_0}k). \quad (3.2)$$

Since $S(\frac{c_0}{a_0}k)=0$ for $|\frac{c_0}{a_0}k|>f_c$, we find that $u(x)$ is spatially band-limited over $(-\frac{a_0}{c_0}f_c, \frac{a_0}{c_0}f_c)$. Furthermore, by the well known sampling theorem, in order to reconstruct $u(x)$ from its samples $u(iD)$, the interval D must satisfy

$$D < \frac{c_0}{2a_0 f_c} = \frac{\lambda_c}{2a_0}, \quad (3.3)$$

where λ_c is the minimum wave length of the signal. Since $a_0 = \sin \theta_0$ is no greater than unity, we get fixed bounds:

$$k_c = \frac{f_c}{c_0} \quad (3.4)$$

and

$$D < \frac{\lambda_c}{2}. \quad (3.5)$$

When $u(x)$ is (spatially) sampled at a rate $1/D$, the sequence $u(iD)$ is band-limited over $(-k_c D, k_c D)$, or $(-\frac{D}{c_0} f_c, \frac{D}{c_0} f_c)$. Thus, Jain's approach can be applied spatially to each group of samples obtained at $2M+1$ sensors at each temporal sampling time. The T 's in Eqn. (2.14) and Eqn. (2.15) are replaced by $\frac{D}{c_0}$'s with D satisfying the same requirement as conventional beamformer, i.e., $D < \frac{\lambda_c}{2}$. A real-time implementation scheme is shown in Fig. 3.1. The truncation point M' of the extrapolation along x -axis will be discussed in section 3.3. From the figure we see that in extending the array length synthetically, we add some multipliers, adders, and registers. This is worthwhile even in comparison with the case where physical sensors are added. This is because with the compatible results (discussed later), the synthetic approach avoids possible long noise-sensitive connection cables between the additional sensors and the central processing unit, and saves sensors and A/D converters as well.

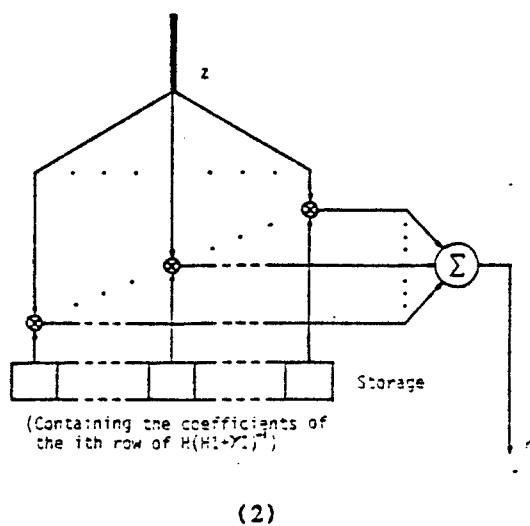
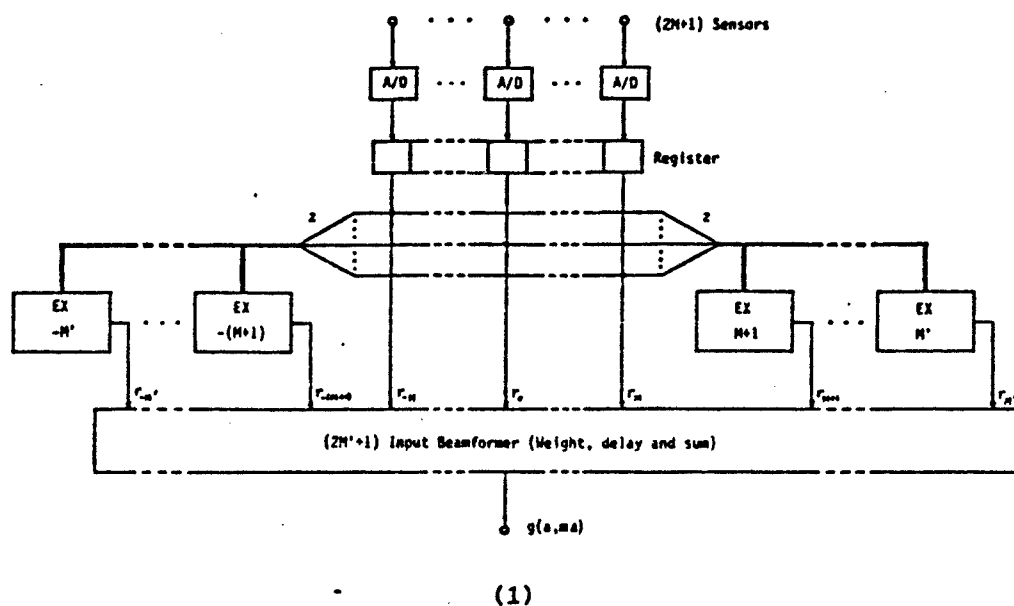


Fig. 3.1 Real-time implementation scheme of an extrapolation beamformer: (1) Overall scheme (2) The i th extrapolator ($EX i$) in (1) for $M+1 \leq i \leq M'$

Other techniques, such as temporal interpolation, sampling techniques for band-limited signals, and frequency domain beamforming [2]-[7], can be used simultaneously with the spatial extrapolation. However, they will not be discussed in this thesis.

3.2 Extrapolation Error

As mentioned earlier, the extrapolated sequences do not in general equal the samples of the original continuous signal which we seek to reconstruct, i.e., there is some "extrapolation error". We also mentioned that these extrapolated sequences converge to those continuous values uniformly if the sampling interval T ($\frac{D}{c_0}$ in our case) approaches zero [13]. Thus, for a relatively small $\frac{D}{c_0}$ we may expect that the extrapolation error is within some bound so that the extrapolation beamforming is meaningful. The quantitative measurement of the error is needed in evaluating the performance of the extrapolation beamformer. Unfortunately, it is very difficult to evaluate these errors analytically for the reason discussed below.

We notice that Jain's formula was obtained earlier through numerical approximation of some integral equations by Cadzow [10]. Specifically, the one-step extrapolation for continuous case is

$$\int_{\tau \in \Lambda} h_1(t-\tau) x(\tau) d\tau = z(t); \quad t \in \Lambda \quad (3.6)$$

$$y(t) = \int_{\tau \in \Lambda} h(t-\tau) x(\tau) d\tau; \quad t \notin \Lambda \quad (3.7)$$

where $h(t)$ and $h_1(t)$ are the impulse response of a low-pass filter with cutoff frequency f_c , $x(t)$ is an intermediate variable, and Λ is the observation interval. One first solves Eqn. (3.6) for $x(t)$ based on the observation $z(t)$, then substitutes the $x(t)$ in Eqn. (3.7) to obtain the result $y(t)$. A numerical approximation to this set of equations is

$$\sum_{j=-M}^M h_1(iT-jT) x(jT) = z(iT); \quad |i| \leq M \quad (3.8)$$

$$y(iT) = \sum_{j=-M}^M h(iT-jT) x(jT) T; \quad |i| > M. \quad (3.9)$$

Note that this set of equations is exactly the same as Eqn. (2.13) where it was written in matrix form. Since Eqn. (3.6) and Eqn. (3.7) reconstruct the continuous signal exactly, the extrapolation error mentioned above is just the numerical approximation error of Eqn. (3.6) and Eqn. (3.7). We now show that it is impractical to evaluate this error. First of all, Eqn. (3.6) may not have a solution at all if $y(t)$ (hence $z(t)$) does not satisfy certain conditions [10], [11]. In this case, although an MNLS solution to Eqn. (3.8) exists, it is meaningless to mention the error. These conditions will not be quoted here, since even if a solution to Eqn. (3.6) does exist, we still cannot estimate the error. This is because the numerical approximation to Eqn. (3.6) (solution of Eqn. (3.8)) can be quite different from the samples of the continuous solution of Eqn. (3.6) due to the ill-posed nature of the Fredholm equation of the first kind. Equation (3.6) can be rewritten as

$$\int_{\tau \in \Lambda} h_1(iT-\tau) x(\tau) d\tau = T \sum_{j=-M}^M h_1(iT-jT) x(jT) + Q(h_1, x, T)$$

$$= z(iT); \quad |i| < M \quad (3.10)$$

where $Q(h_1, x, T)$ denotes the non-zero remainder. Equation (3.8), however, is the above equation with $Q(h_1, x, T)=0$. Thus, Eqn. (3.8) actually solves another integral equation

$$\int_{\tau \in \Lambda} h_1(iT-\tau) \hat{x}(\tau) d\tau = T \sum_{j=-M}^M h_1(iT-jT) \hat{x}(jT) + Q(h_1, \hat{x}, T)$$

$$= z(iT) + Q(h_1, \hat{x}, T); \quad |i| < M \quad (3.11)$$

with $Q(h_1, \hat{x}, T) \neq 0$. By the argument in [16], we see that the small perturbation $Q(h_1, \hat{x}, T)$ on the right hand side of Eqn. (3.11) causes the solution $\hat{x}(\tau)$ to move arbitrarily far from desired $x(\tau)$. Hence, the error $\hat{x}(jT) - x(jT)$ cannot be predicted, let alone the error of $y(jT)$ in Eqn. (3.9).

A practical approach to this problem is to conduct some numerical experiments with example signal sequences, and then to model the error obtained from the experiments. This has in fact been done, and the main results are presented below. The method used to invert the matrix $(H_1 + \gamma I)$ in Jain's formula is the well-known Gauss elimination method which gives more accurate and more reliable results than other methods

such as Levinson's algorithm. The computation time is not important because the coefficients of $H(HI + \gamma I)^{-1}$ need to be calculated only once before the installation of the equipment. A sum of two shifted sinc functions (called SHSINC) and a sine function (SINE) are used as signals. Although the latter has not been proven to converge to continuous solutions, Jain's approach still gives a good results as shown below. The observation is made at 17 points, i.e., $M=8$. The quantity $f_{\frac{D}{c_0}}$ is the digital cutoff frequency F , which is less than 0.5 (since $D < \frac{c_0}{2f_c}$). The digital signal frequency $f_{\frac{D}{c_0}}$, denoted by F_1 (for SHSINC, it is the highest frequency of the sinc function), is less than or equal to F .

First, we investigate the noise-free case, i.e., $N=0$. In a practical situation, the signal sequences may have several degrees of freedom. Their frequencies as well as their phases may vary. We now look at the extrapolation error for different phase shifts. It is observed for SINE shifting from 0 to 2π . For SHSINC, the separation points between two main peaks is 60, the shift is from the -150th point to the 50th point. The filter cutoff frequency is 0.05 if it is not specified. Dashed lines are signals, and solid lines are error if not otherwise indicated.

Figure 3.2 and Fig. 3.3 show the extrapolation error vs. x/D for SHSINC and SINE respectively when their shifts are all zero. We can see a flat region in the central part of the extrapolation error, indicating that good extrapolation almost doubles the observation length. Notice that γ is not zero as it should be in ideal noise-free case. This is because experimentally, very poor extrapolation results if $\gamma=0$, due to

SHSINC
 (2M-1)=17
 SHIFT=0
 F=.05
 F1=.04
 SNR=110.

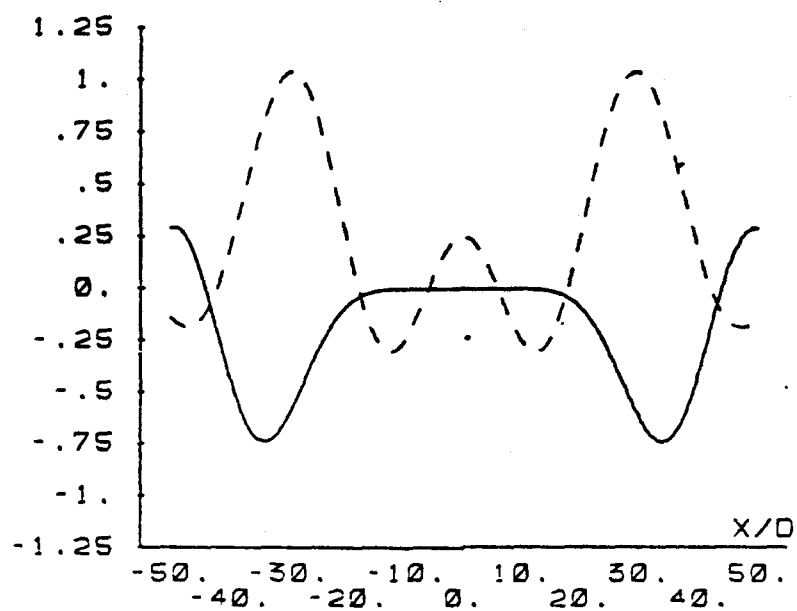


Fig. 3.2 Extrapolation error vs. i for SHSINC

SINE
 (2M-1)=17
 SHIFT=PI*0.
 F=.05
 F1=.04
 SNR(DB)=110.

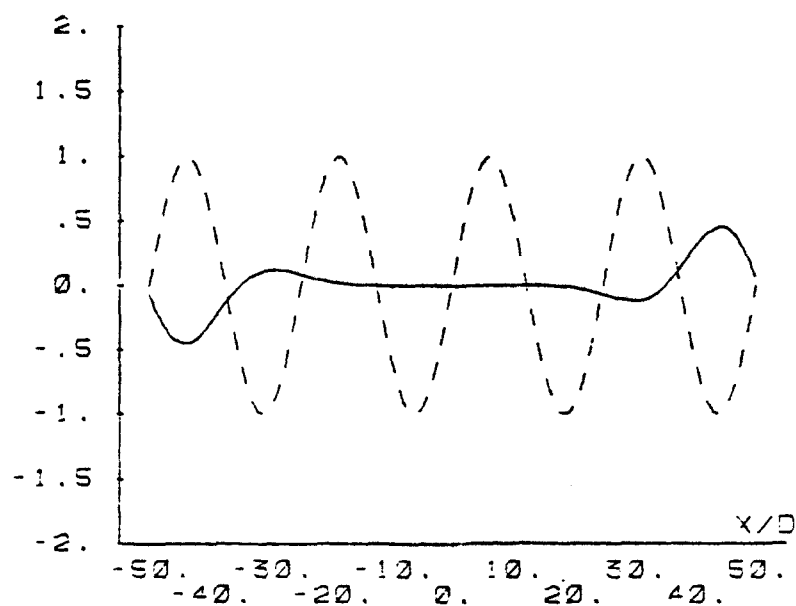


Fig. 3.3 Extrapolation error vs. i for SINE

the ill-conditionness of the matrix H_1 and the round off error in computation. This problem is solved by adding a very small number to the diagonal of H_1 to "stabilize" it [12], which is exactly the same as letting γ equal this small number (in our case 10^{-11} to 10^{-12} is enough) in Eqn. (2.17) for $N=0$.

Next we fix i ($i=x/D$) at a point, let the signal shift in aforementioned ranges, and observe the extrapolation error vs. shift for this particular point of i . The plots for SHSINC are shown in Fig. 3.4 through Fig. 3.7 for different i and different F_1 . It is interesting to see that the error is almost a shifted version of the signal with the magnitude multiplied by a negative number. It is also observed that this model fits better for low signal frequency case ($F_1=0.02$). Figure 3.8 through Fig. 3.13 show same plots for SINE. We observe that in these cases the error is exactly sinusoidal with one complete cycle. As F_1 increases to F , its magnitude becomes larger, and its shift with respect to the signal becomes irregular (see Fig. 3.12 and Fig. 3.13, the shifts are not 180° as it is for smaller F_1 case).

The magnitude of the peak error for these shift ranges at each point of i is shown in Fig. 3.14 through Fig. 3.18 for different cases (since this magnitude is symmetric, only one half is shown). It is clearly seen that

- (1) For the signal of SINE, the error becomes very large when F_1 equals F while it remains small even for $F_1=0.96F$. This phenomenon is not observed for SHSINC. This is because the spectrum of SINE is an

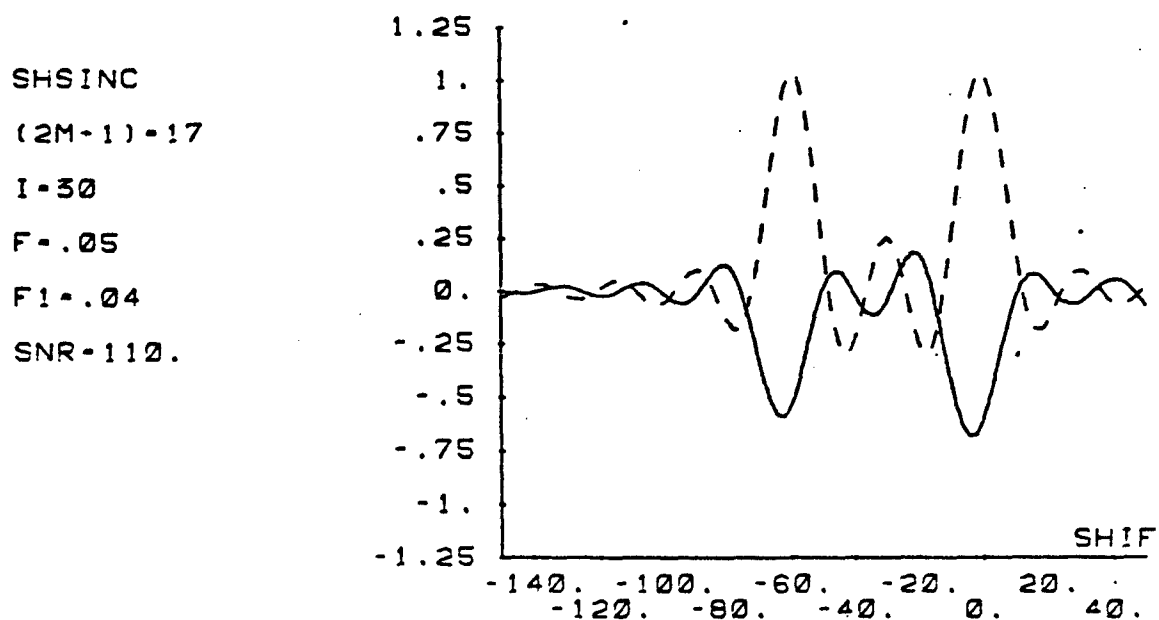


Fig. 3.4 Extrapolation error vs. shift for SHSINC, $\gamma=10^{-11}$, $F1=0.04$, $x=300$

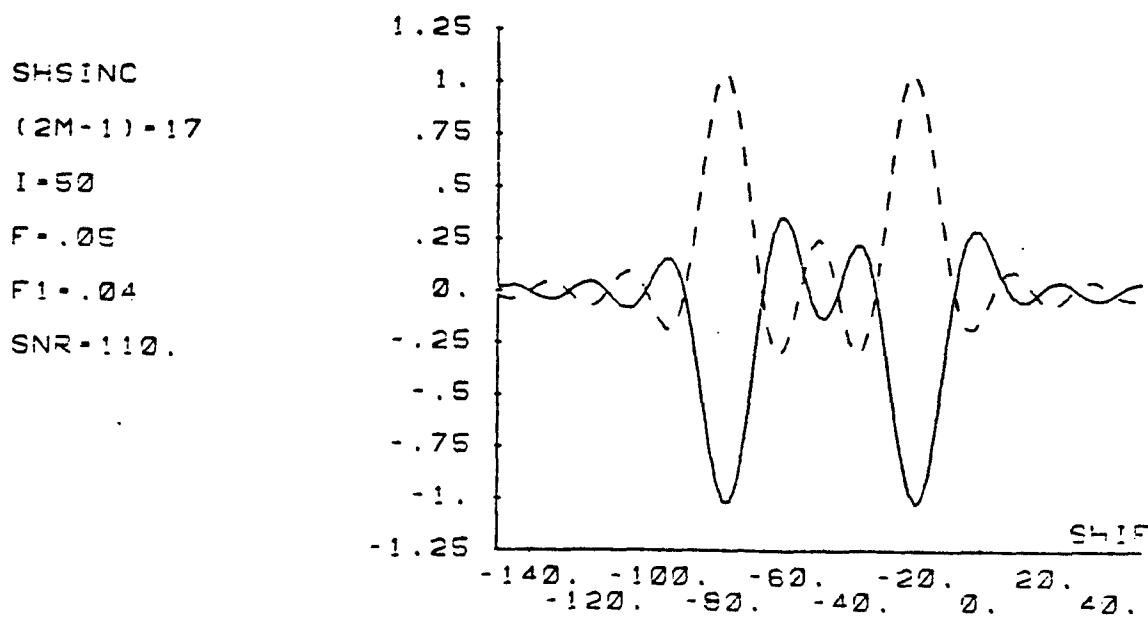


Fig. 3.5 Extrapolation error vs. shift for SHSINC, $\gamma=10^{-11}$, $F1=0.04$, $x=500$

SHSINC
 $(2M-1)=17$
 $I=30$
 $F=.05$
 $F1=.02$
 $SNR=110.$

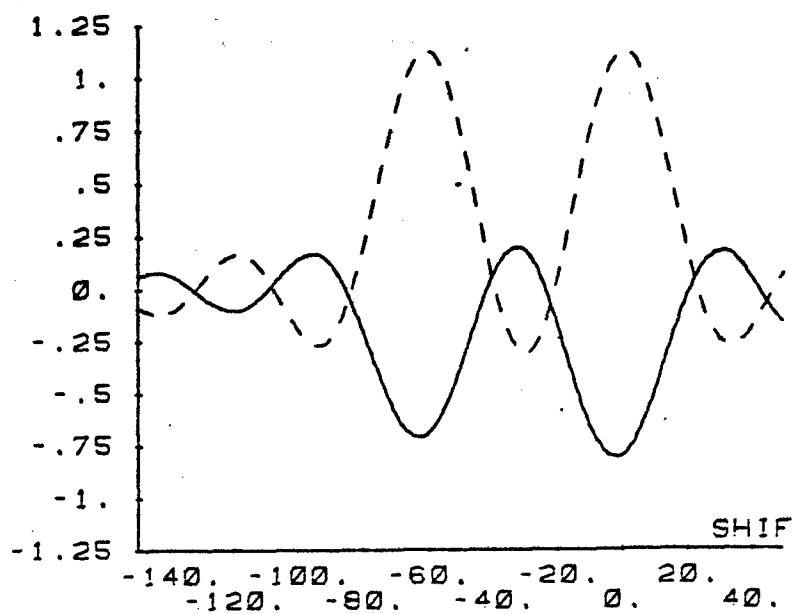


Fig. 3.6 Extrapolation error vs. shift for SHSINC, $\gamma=10^{-11}$, $F1=0.02$, $x=30D$

SHSINC
 $(2M-1)=17$
 $I=50$
 $F=.05$
 $F1=.02$
 $SNR=110.$

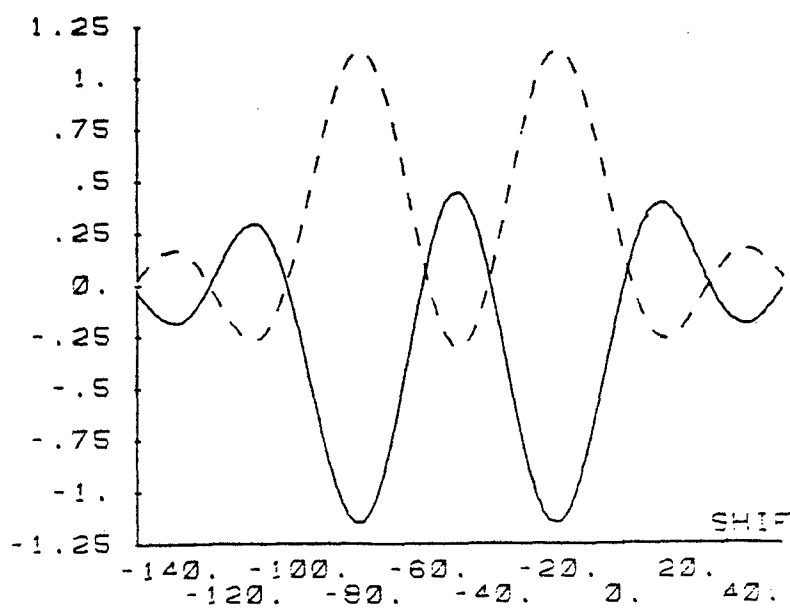


Fig. 3.7 Extrapolation error vs. shift for SHSINC, $\gamma=10^{-11}$, $F1=0.02$, $x=50D$

SINE
 (2M-1)=17
 I=30
 F=.05
 F1=.02
 SNR(DB)=110.

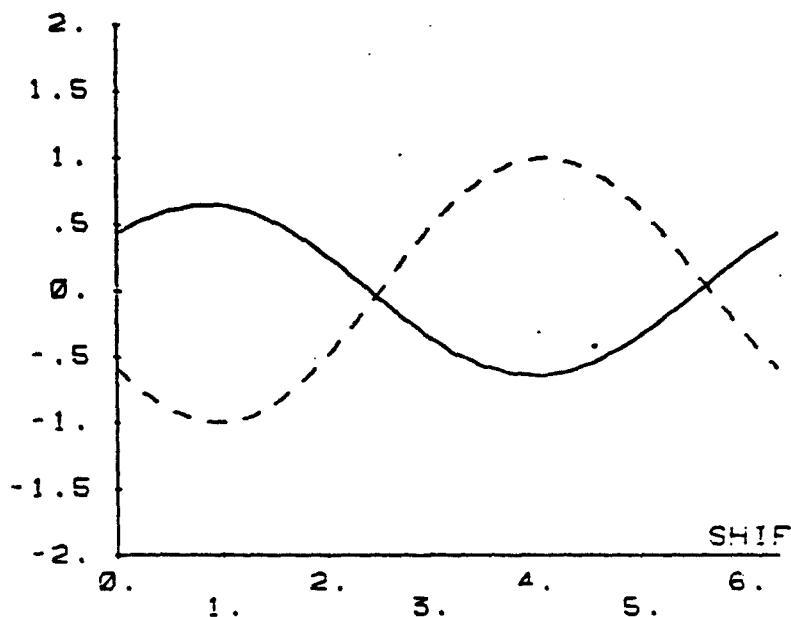


Fig. 3.8 Extrapolation error vs. shift for SINE, $\gamma=10^{-11}$, $F1=0.02$, $x=300$

SINE
 (2M-1)=17
 I=50
 F=.05
 F1=.02
 SNR(DB)=110.

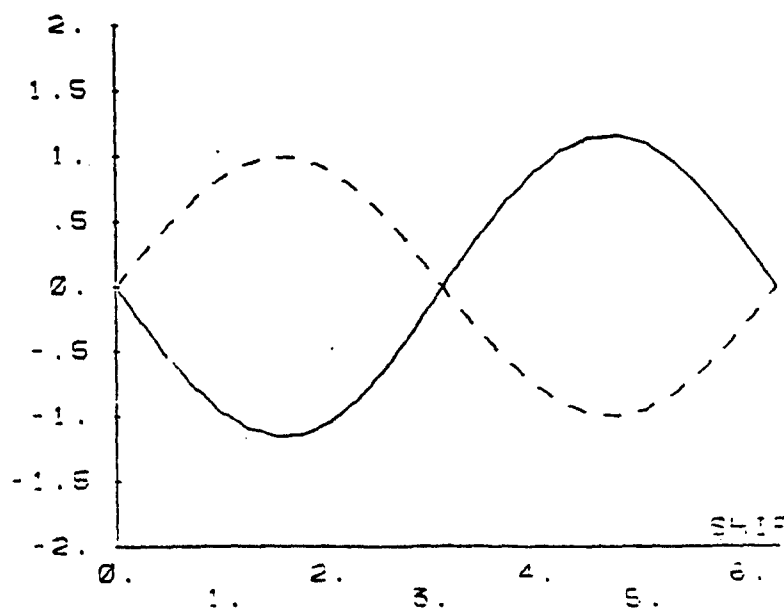


Fig. 3.9 Extrapolation error vs. shift for SINE, $\gamma=10^{-11}$, $F1=0.02$, $x=500$

SINE
 (2M-1)=17
 I=30
 F=.05
 F1=.04
 SNR(DB)=110.

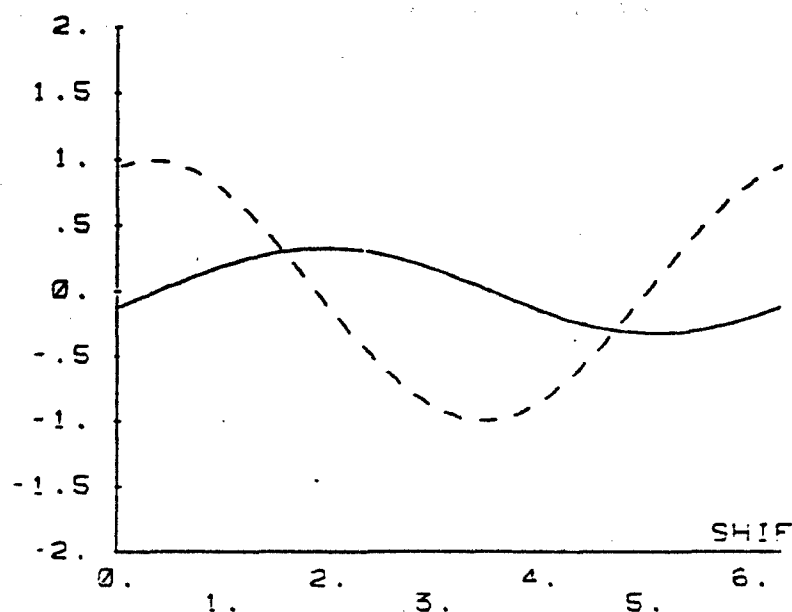


Fig. 3.10 Extrapolation error vs. shift for SINE, $\gamma=10^{-11}$, $F1=0.04$, $x=30D$

SINE
 (2M-1)=17
 I=50
 F=.05
 F1=.04
 SNR(DB)=110.

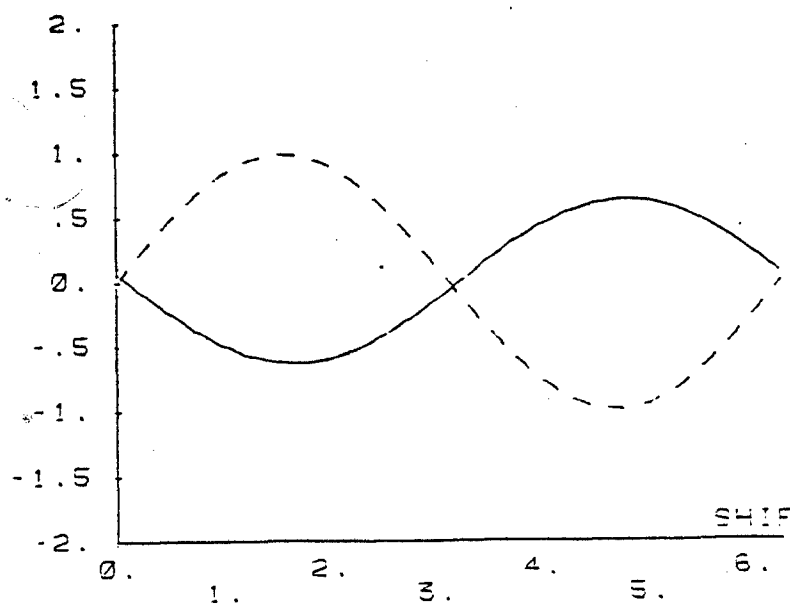


Fig. 3.11 Extrapolation error vs. shift for SINE, $\gamma=10^{-11}$, $F1=0.04$, $x=50D$

SINE
 (2M-1)=17
 I=30
 F=.05
 F1=.05
 SNR(DB)=110.

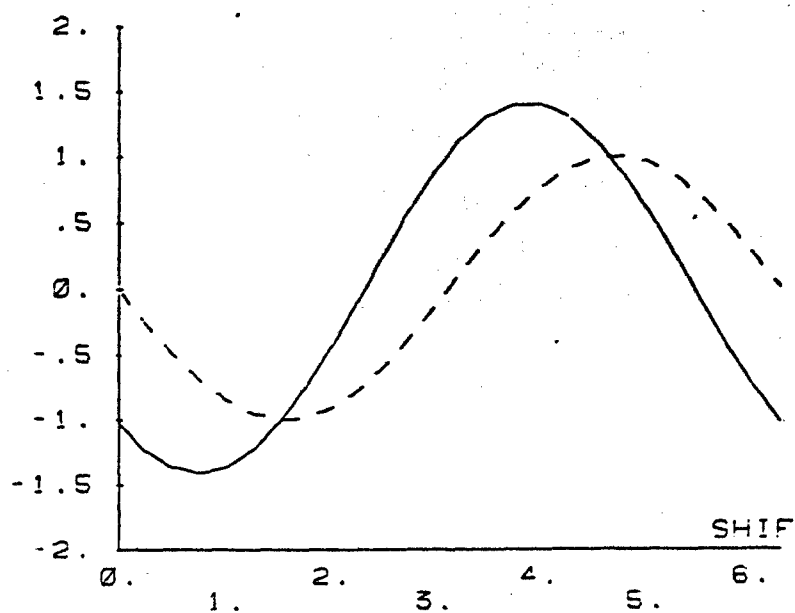


Fig. 3.12 Extrapolation error vs. shift for SINE, $\gamma=10^{-11}$, $F1=0.05$, $x=30D$

SINE
 (2M-1)=17
 I=50
 F=.05
 F1=.05
 SNR(DB)=110.

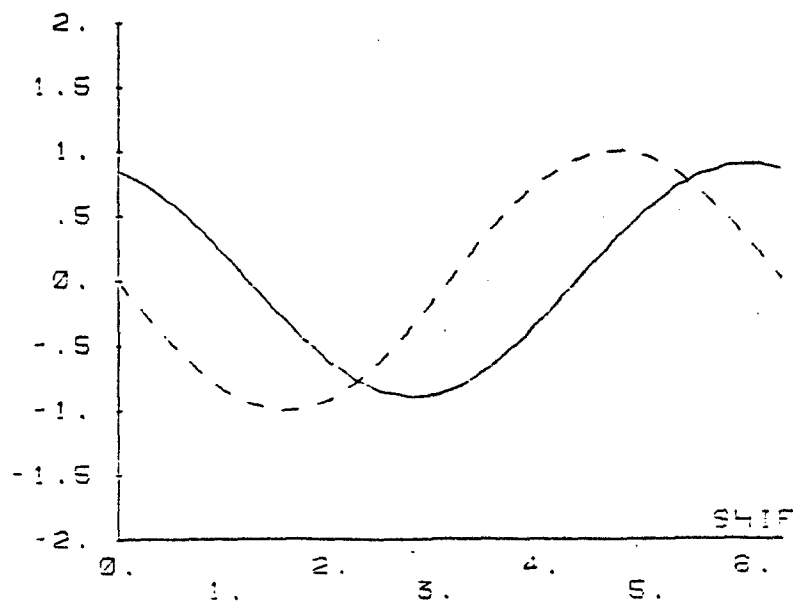


Fig. 3.13 Extrapolation error vs. shift for SINE, $\gamma=10^{-11}$, $F1=0.05$, $x=50D$

SHSINC
 $F = .05$
 $(2M-1) = 17$
 $SNR = 110.$
 1. $F1 = 0.0$
 2. $F1 = 0.4F$
 3. $F1 = 0.8F$
 4. $F1 = 0.96F$
 5. $F1 = F$

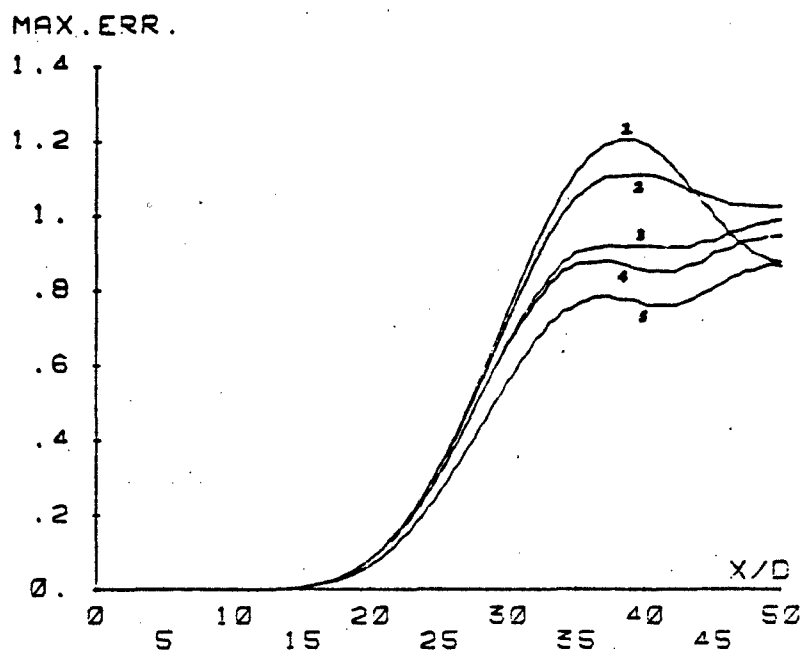


Fig. 3.14 Magnitude of extrapolation error vs. i for SHSINC, $\gamma = 10^{-11}$, $F = 0.05$

SHSINC
 $F = .1$
 $(2M-1) = 17$
 $SNR = 110.$
 1. $F1 = 0.0$
 2. $F1 = 0.4F$
 3. $F1 = 0.8F$
 4. $F1 = 0.96F$
 5. $F1 = F$

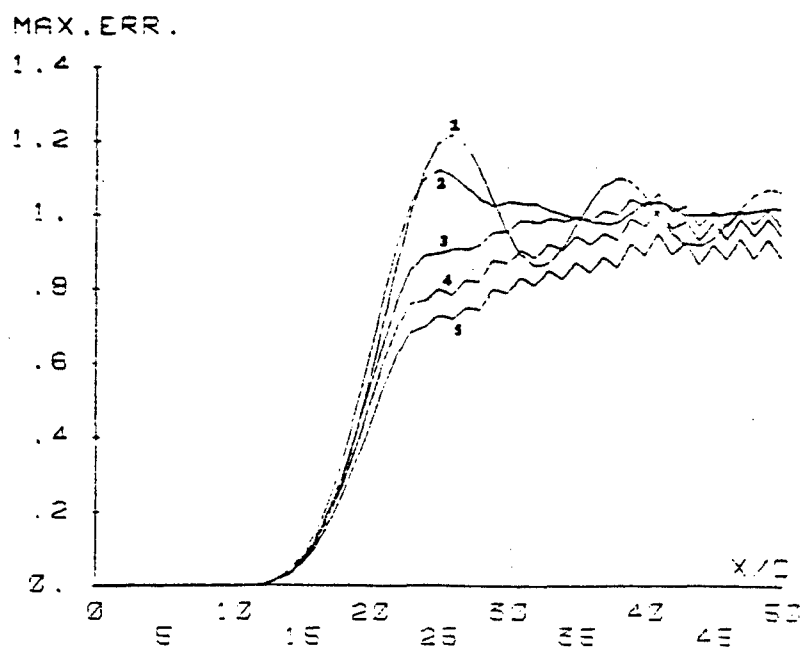


Fig. 3.15 Magnitude of extrapolation error vs. i for SHSINC, $\gamma = 10^{-11}$, $F = 0.1$

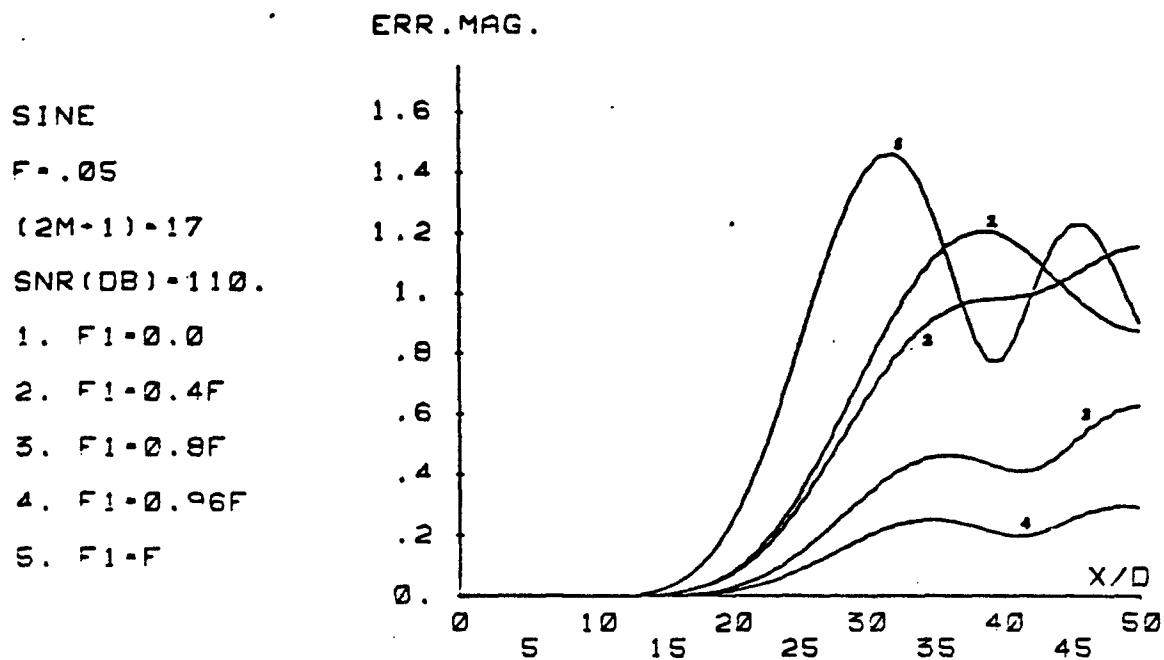


Fig. 3.16 Magnitude of extrapolation error vs. i for SINE, $\gamma = 10^{-11}$, $F = 0.05$

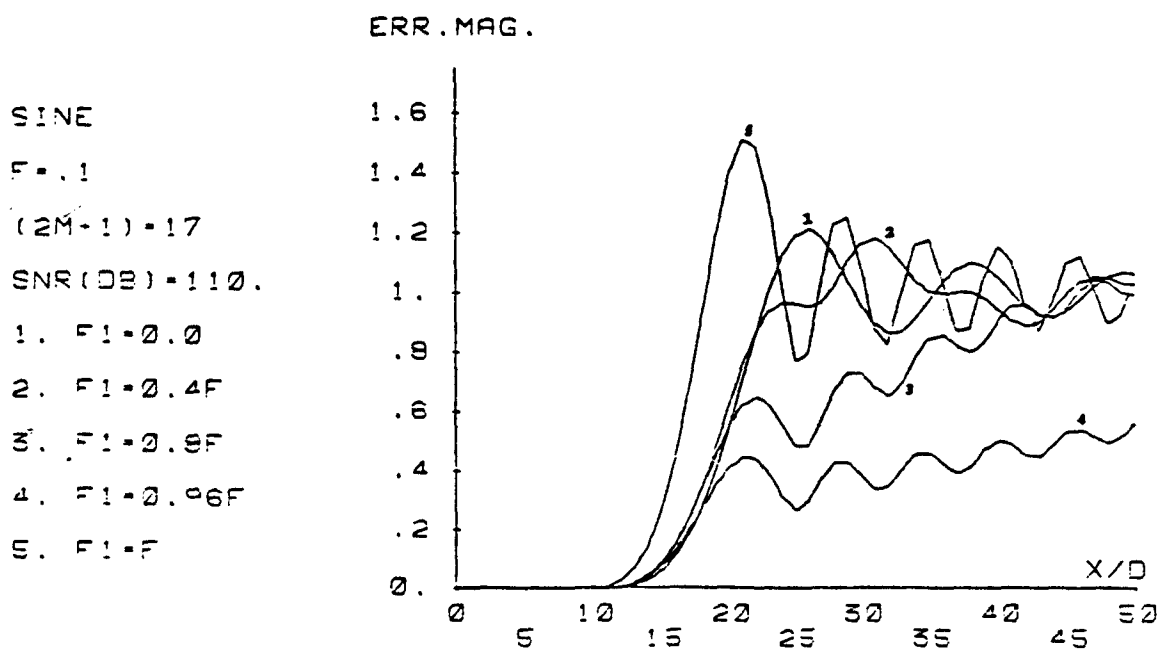


Fig. 3.17 Magnitude of extrapolation error vs. i for SINE, $\gamma = 10^{-11}$, $F = 0.1$

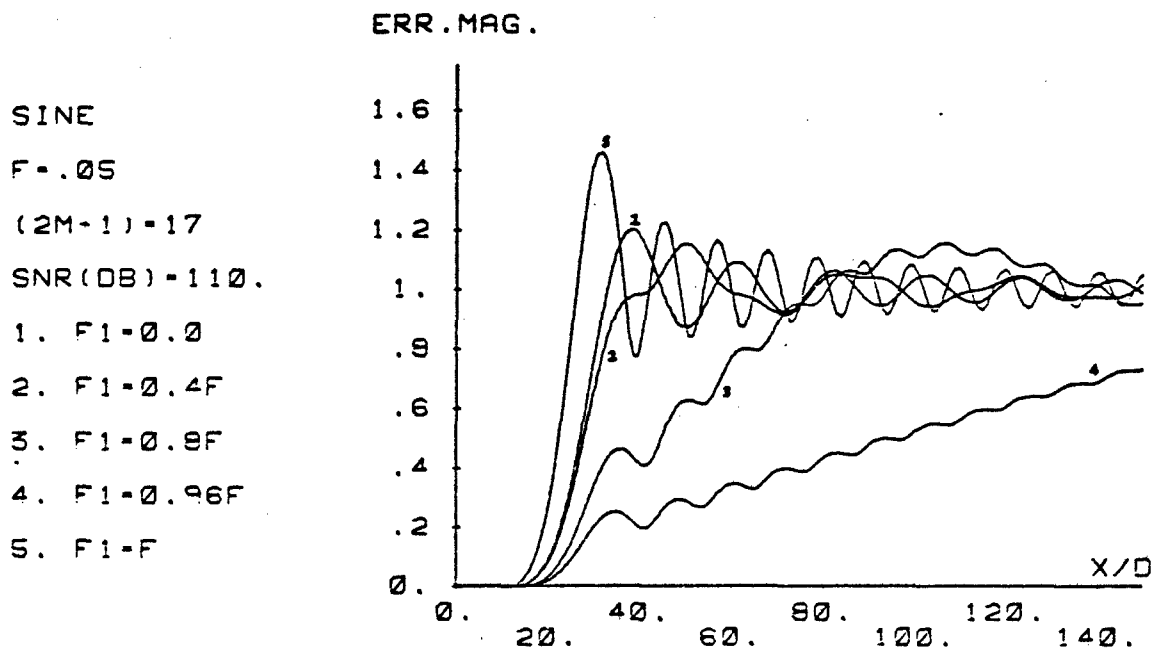


Fig. 3.18 Long tail view of error magnitude vs. i for SINE, $\gamma = 10^{-11}$, $F = 0.05$

impulse, and if it equals the cutoff frequency of the low-pass filter, it is almost cut off by the filter. While the spectrum of SHSINC extends from zero to F_1 , thus no information is lost even if F_1 equals F .

- (2) For a fixed F_1 , smaller filter frequency F (but still larger than F_1) achieves better extrapolation in the sense that the error is smaller (e.g., compare the curve of $F_1=0.04$ in Fig. 3.16 with the curve of same F_1 in Fig. 3.17).
- (3) The extrapolation error tends to unity when i increases as shown in Fig. 3.18. This is because the extrapolated sequence tends to zero as i increases.

Since SINE signal is a basis for any other signals via Fourier transform, and also exhibits a better property in extrapolation in the sense that the error vs. shift is an exact sine function, we will concentrate on the extrapolation and beamforming problems for the sine signal only.

Suppose the sine signal has a random phase θ which is uniformly distributed on $[0, 2\pi]$, i.e., $y(x) = \sin(\Omega x + \theta)$, then by the above observation we can model the error at a fixed i as

$$E(x, \theta) = E(iD, \theta) = -A(i) \sin(\Omega iD + \theta) \quad (3.12)$$

so that the error and the signal are 180° out of phase for each x . The magnitude function $A(i)$ can be obtained by curve-fitting the plots of magnitude vs. i . It is easy to calculate the density function of E at

each i

$$f_E = \begin{cases} \frac{1}{\pi \sqrt{A^2(x) - E^2}} ; |E| < A(x) \\ 0 & ; \text{otherwise.} \end{cases} \quad (3.13)$$

From observation (1) above and from the earlier observation about error vs. shift we see that the filter cutoff frequency f_c (hence F) should be larger than maximum possible signal frequency f ($F1$). On the other hand, observation (2) implies that it is better that F is small. Thus, in a practical situation, we need to estimate the maximum signal frequency f and select f_c and D ($F = f_c \frac{D}{c_0}$) carefully to trade off between these two aspects.

Now let us consider the noisy case. For uncorrelated white Gaussian noise N added to the observation, we have

$$Z = Z_1 + N \quad (3.14)$$

where $Z_1 = PY$, and

$$\begin{aligned} \hat{Y} &= H(H1 + \gamma I)^{-1} Z \\ &= H(H1 + \gamma I)^{-1} (Z_1 + N) \\ &= H(H1 + \gamma I)^{-1} Z_1 + H(H1 + \gamma I)^{-1} N. \end{aligned} \quad (3.15)$$

Thus \hat{Y} can be expressed as a sum of two terms

$$\hat{Y} = \hat{Y}_d + \hat{Y}_r \quad (3.16)$$

where

$$\hat{Y}_d = H(HI + \gamma I)^{-1} Z_1 \quad (3.17)$$

$$\hat{Y}_r = H(HI + \gamma I)^{-1} N. \quad (3.18)$$

Notice that \hat{Y} , \hat{Y}_d and \hat{Y}_r are all infinite-dimensional vectors while Z_1 and N are $(2M+1) \times 1$ vectors. We see that each element of \hat{Y}_r is a linear combination of that of N , hence \hat{Y}_r is also white and Gaussian. The analysis for \hat{Y}_d is exactly the same as before except that γ is much larger. An arbitrary value for γ is chosen so that $10 \log_{10} \frac{1}{\gamma}$ is 13 dB (This value will be used throughout the thesis if it is not otherwise specified).

The plots for error vs. phase shift are shown in Fig. 3.19 through Fig. 3.28. We see that the error coincides with the signal (with 180° out of phase) better than $N=0$ case for F_1 less than $0.8F$. Beyond $F_1=F$, the error does not fit into the model well. The error magnitude vs. i is plotted in Fig. 3.29 and Fig. 3.30 for $0 \leq i \leq 50$ ($A(i)$ is symmetric). We see also that the error gets larger for F_1 beyond $0.8F$. Thus, in designing an extrapolation beamformer, we should choose f_c such that

$$0.8f_c > f_{\max}. \quad (3.19)$$

SINE
 $(2M-1)=17$
 $I=14$
 $F=.05$
 $F1=.04$
 $SNR(DB)=13.$

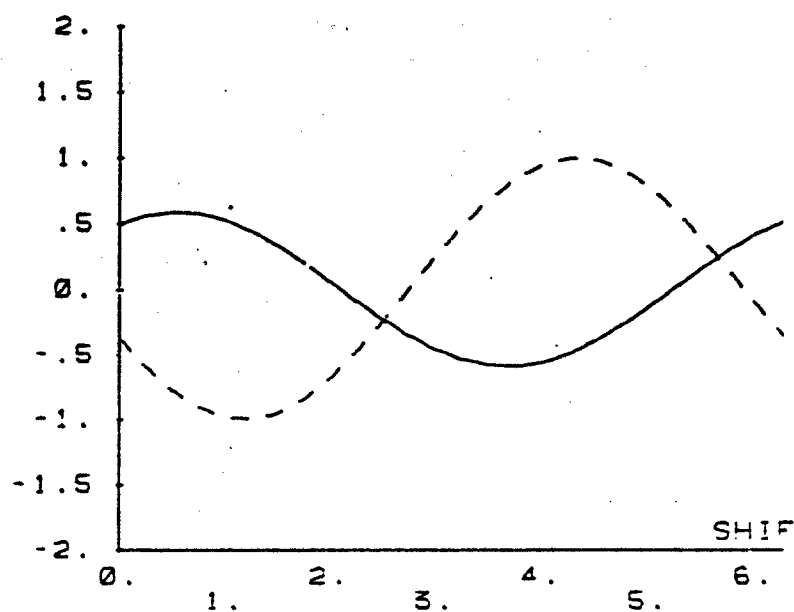


Fig. 3.19 Extrapolation error vs. shift for SINE, $\gamma=0.05$, $F1=0.04$, $x=14D$

SINE
 $(2M-1)=17$
 $I=25$
 $F=.05$
 $F1=.04$
 $SNR(DB)=13.$

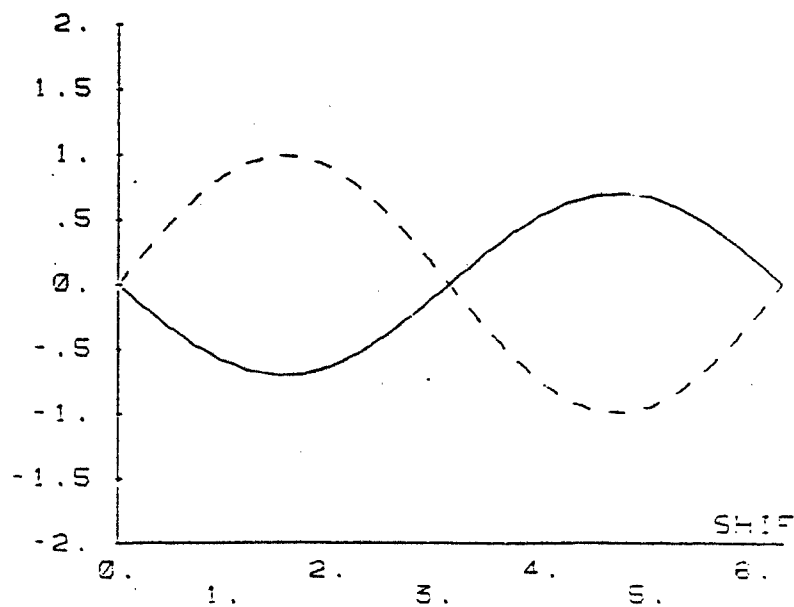


Fig. 3.20 Extrapolation error vs. shift for SINE, $\gamma=0.05$, $F1=0.04$, $x=25D$

SINE
 $(2M-1)=17$
 $I=18$
 $F=.05$
 $F1=.03$
 $SNR(DB)=13.$

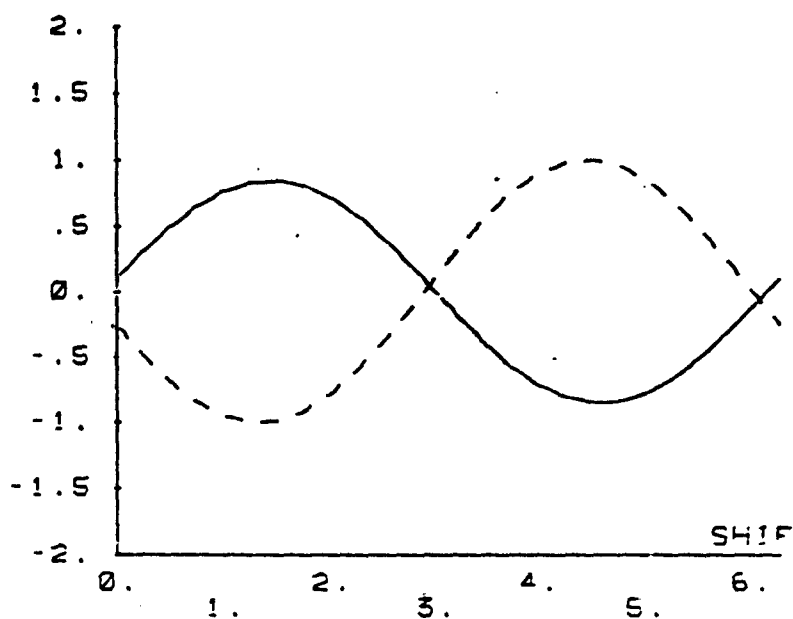


Fig. 3.21 Extrapolation error vs. shift for SINE, $\gamma=0.05$, $F1=0.03$, $x=18D$

SINE
 $(2M-1)=17$
 $I=33$
 $F=.05$
 $F1=.03$
 $SNR(DB)=13.$

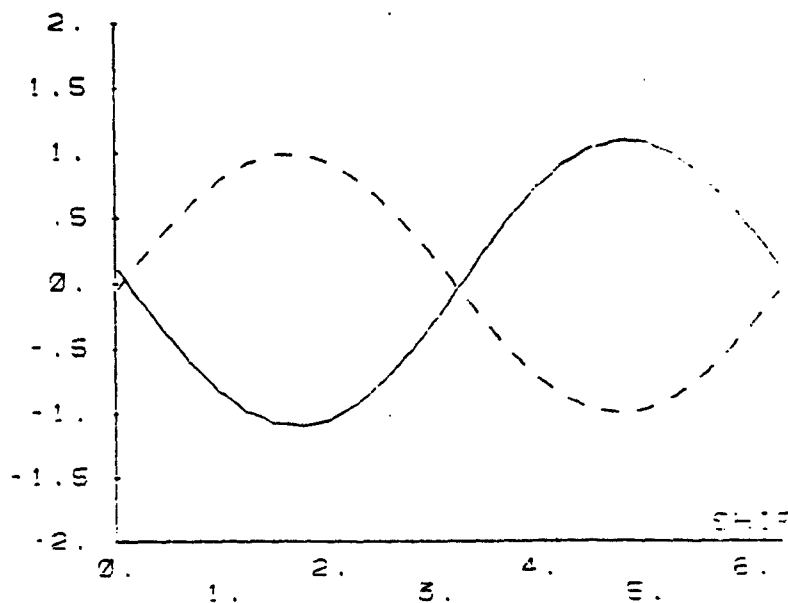


Fig. 3.22 Extrapolation error vs. shift for SINE, $\gamma=0.05$, $F1=0.03$, $x=33D$

SINE
 $(2M-1)=17$
 $I=15$
 $F=.05$
 $F1=.02$
 $SNR(DB)=13.$

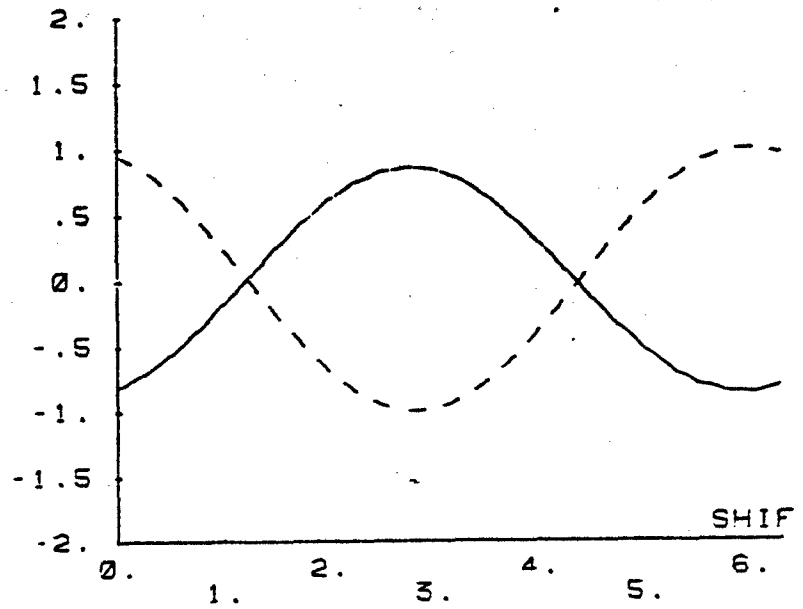


Fig. 3.23 Extrapolation error vs. shift for SINE, $\gamma=0.05$, $F1=0.02$, $x=15D$

SINE
 $(2M-1)=17$
 $I=25$
 $F=.05$
 $F1=.02$
 $SNR(DB)=13.$

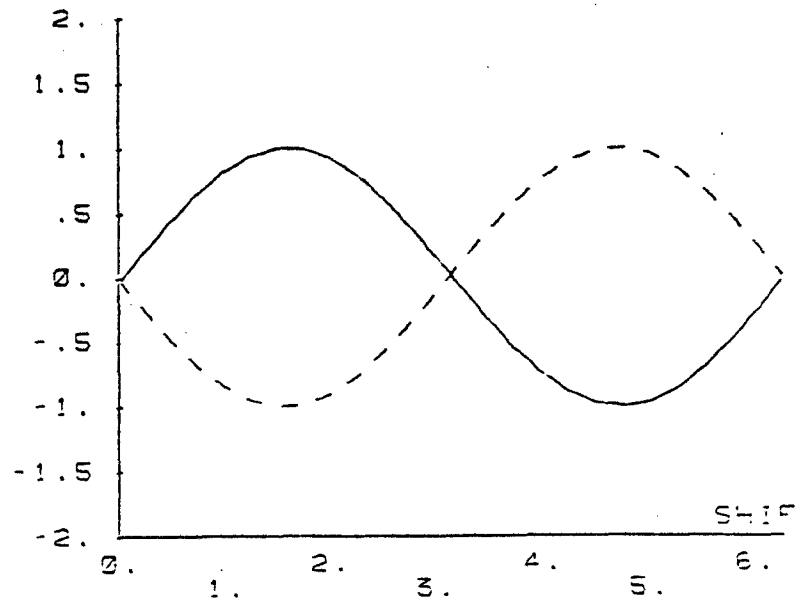


Fig. 3.24 Extrapolation error vs. shift for SINE, $\gamma=0.05$, $F1=0.02$, $x=25D$

SINE
 $(2M-1)=17$
 $I=50$
 $F=.05$
 $F1=.02$
 $SNR(DB)=13.$

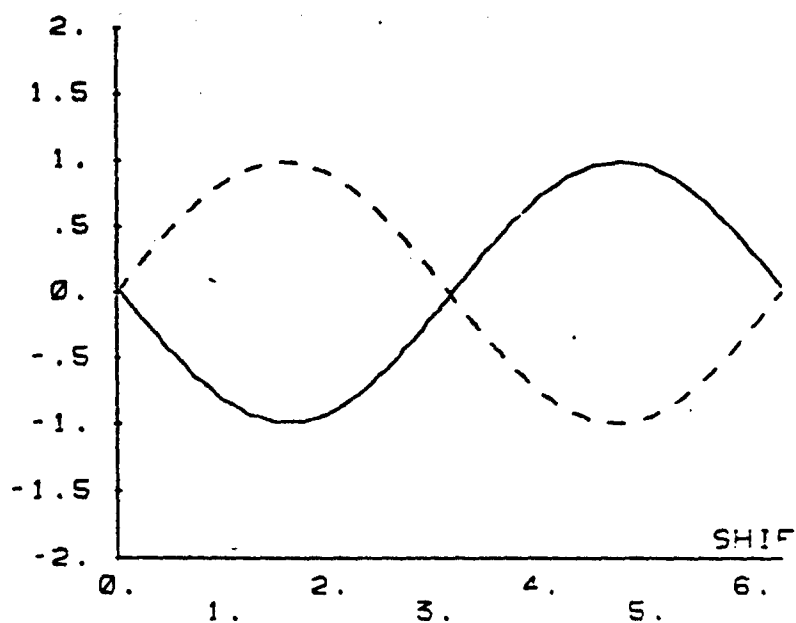


Fig. 3.25 Extrapolation error vs. shift for SINE, $\gamma=0.05$, $F1=0.02$, $x=50D$

SINE
 $(2M-1)=17$
 $I=22$
 $F=.05$
 $F1=.045$
 $SNR(DB)=13.$

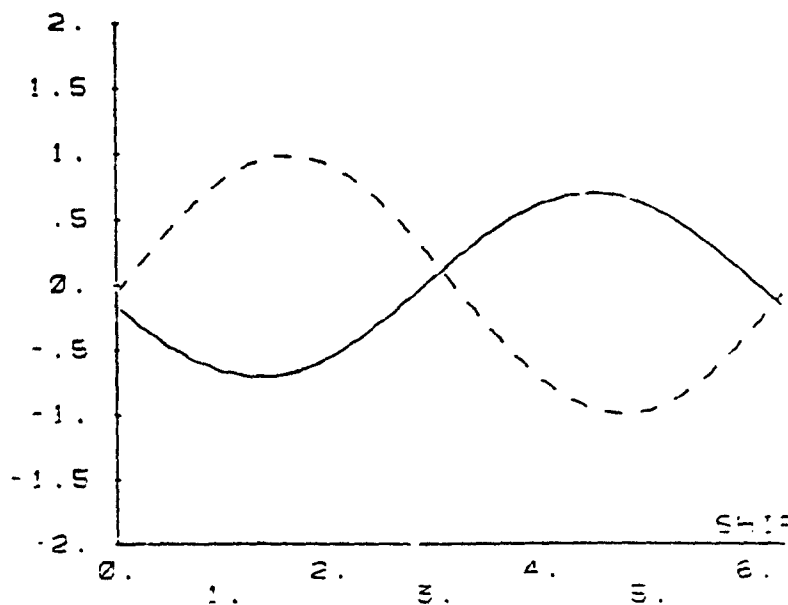


Fig. 3.26 Extrapolation error vs. shift for SINE, $\gamma=0.05$, $F1=0.045$, $x=22D$

SINE
 $(2M-1)=17$
 $I=21$
 $F=.05$
 $F1=.048$
 $SNR(DB)=13.$

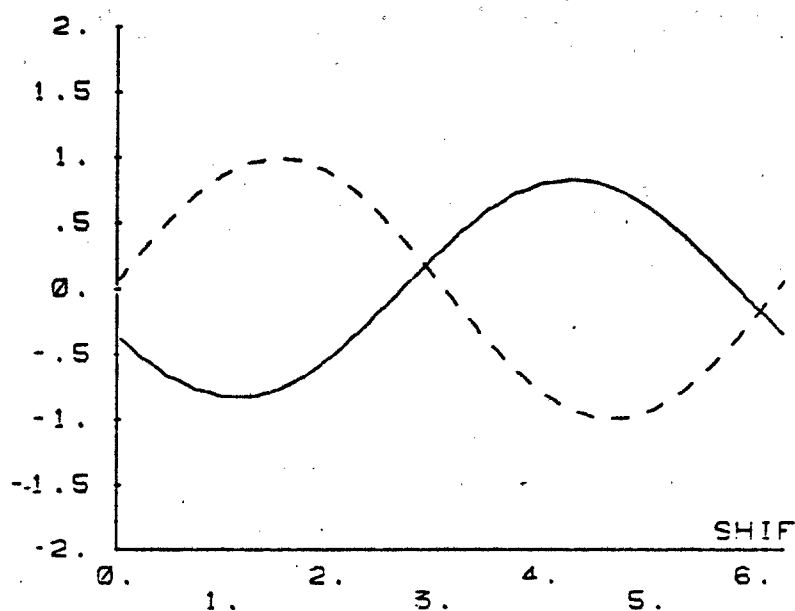


Fig. 3.27 Extrapolation error vs. shift for SINE, $\gamma=0.05$, $F1=0.048$, $x=21D$

SINE
 $(2M-1)=17$
 $I=20$
 $F=.05$
 $F1=.05$
 $SNR(DB)=13.$

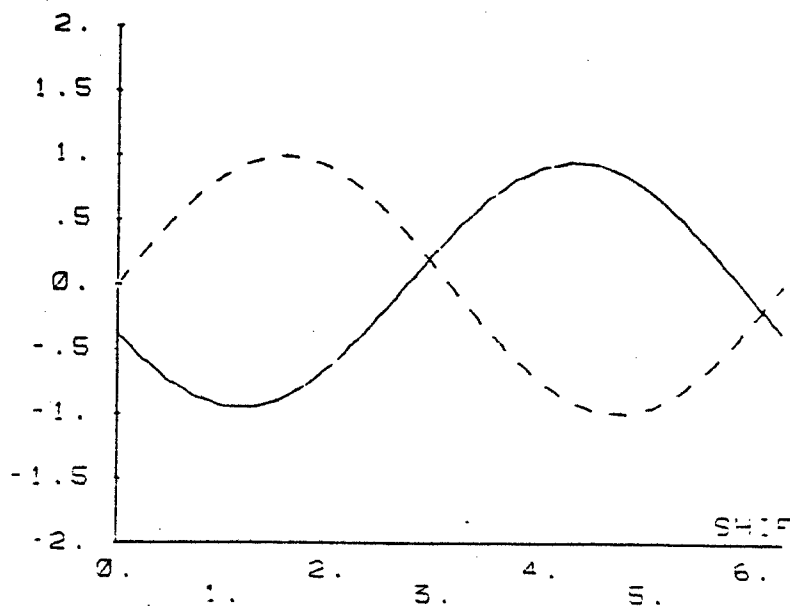


Fig. 3.28 Extrapolation error vs. shift for SINE, $\gamma=0.05$, $F1=0.05$, $x=20D$

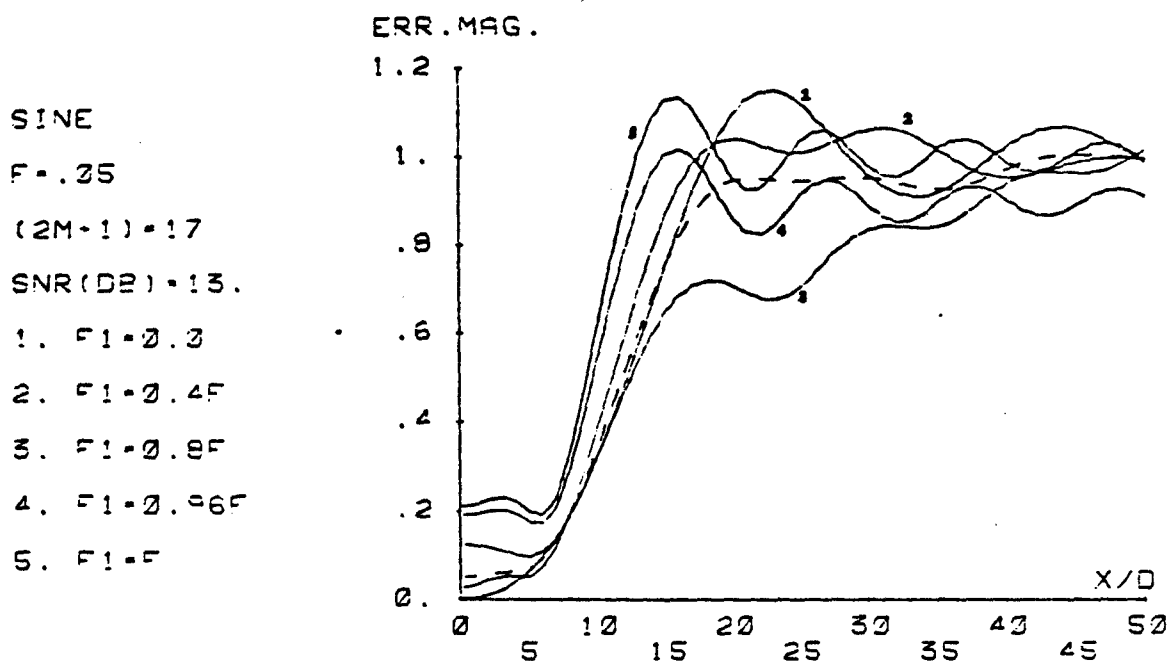


Fig. 3.29 Magnitude of extrapolation error vs. i for SINE, $\gamma=0.05$, $F=0.05$

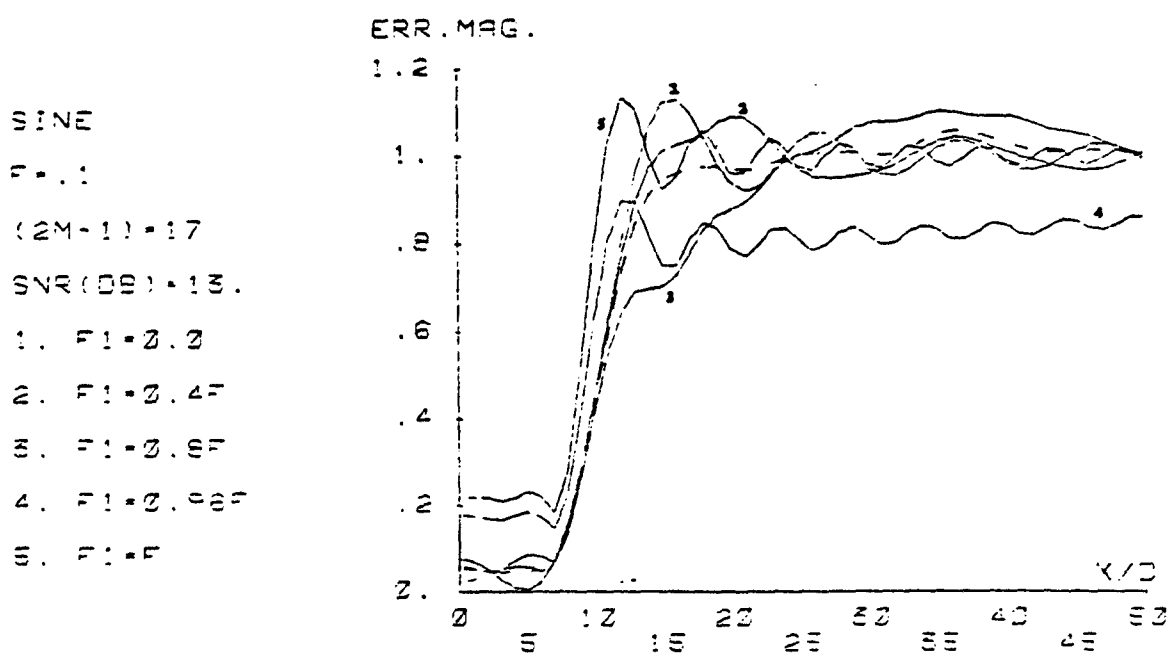


Fig. 3.30 Magnitude of extrapolation error vs. i for SINE, $\gamma=0.05$, $F=0.1$

Thus in these two plots, discarding the curves for $F_1 > 0.8F$, the remaining three curves ($F_1=0$, $F_1=0.4F$ and $F_1=0.8F$) are averaged and are plotted with the dashed lines. They will be used in Section 3.3 and in Chapter 4 as the magnitude function $A(i)$ in the error model (Eqn. (3.12)).

Notice that in Fig. 3.1, the input to the beamformer for $|i| < M$ is fed directly from the sensors without extrapolation. This is because we want to use as much real information as possible. Thus the elements of \hat{Y} for $|i| < M$ are replaced by those of Z and $A(i)$ is set to zero for $|i| < M$. This will not affect the extrapolation for $|i| > M$.

3.3 Evaluation Of Performance

At this stage we are ready to evaluate the performance of the digital extrapolation beamformer using the error model obtained in last section. Specifically, for a sinusoidal incoming wave

$$s(t, x) = \sin\left[\omega_0 \left(t + \frac{x a_0}{c_0}\right) + \phi\right] \quad (3.20)$$

with a random phase uniformly distributed over $[0, 2\pi]$, the i th sensor receives

$$r_i(t, iD) = \sin\left[\omega_0 \left(t + \frac{i D a_0}{c_0}\right) + \phi\right] + n_i(t); \quad |i| < M \quad (3.21)$$

where $n_i(t)$ is the aforementioned noise. After temporal sampling, these x_i 's form the observation vector Z , or the elements of \hat{Y} (denoted \hat{y}_i) for $|i| \leq M$, i.e.,

$$\hat{y}_i(m\Delta, 1D) = \sin\left[\omega_0\left(m\Delta + \frac{1Da}{c_0}\right) + \phi\right] + n_i(m\Delta);$$

$$|i| \leq M. \quad (3.22)$$

Then they are extrapolated to $|i| = M'$, i.e.,

$$\hat{y}_i(m\Delta, 1D) = \sin\left[\omega_0\left(m\Delta + \frac{1Da}{c_0}\right) + \phi\right] - A(i) \sin\left[\omega_0\left(m\Delta + \frac{1Da}{c_0}\right) + \phi\right]$$

$$+ \hat{n}_i(m\Delta);$$

$$M+1 \leq |i| \leq M' \quad (3.23)$$

where $\hat{n}_i(m\Delta)$ is the extrapolated noise, i.e., the i th element of the vector \hat{Y}_r for $M+1 \leq |i| \leq M'$.

All these $2M'+1$ elements of \hat{Y} are fed to the beamformer which gives an output as follows:

$$g(a, m\Delta) = \frac{1}{2M'+1} \sum_{i=-M'}^{M'} \sin\left[\omega_0\left[m\Delta - 1D\left(\frac{a}{c} - \frac{a_0}{c_0}\right)\right] + \phi\right]$$

$$- \frac{1}{2M'+1} \sum_{i=\pm(M+1)}^{\pm M'} A(i) \sin\left[\omega_0\left[m\Delta - 1D\left(\frac{a}{c} - \frac{a_0}{c_0}\right)\right] + \phi\right]$$

$$+ \frac{1}{2M'+1} \sum_{i=-M'}^{M'} \tilde{n}_i\left(m\Delta - \frac{1Da}{c}\right) \quad (3.24)$$

where

$$\tilde{n}_1(m\Delta) = \begin{cases} n_1(m\Delta); & |i| < M \\ \hat{n}_1(m\Delta); & M+1 < |i| < M' \end{cases} \quad (3.25)$$

and

$$\sum_{i=\pm(M+1)}^{\pm M'} = \sum_{i=M+1}^{M'} + \sum_{i=-(M+1)}^{-M'} \quad (3.26)$$

We now evaluate two major measurements: beam pattern and signal-to-noise ratio.

3.3.1 Beam Pattern

Without considering the noise, Eqn. (3.24) becomes

$$\begin{aligned} g(a, m\Delta) &= \frac{1}{2M'+1} \sum_{i=-M'}^{M'} \sin\{\omega_0[m\Delta - iD(\frac{a}{c} - \frac{a_0}{c_0})] + \phi\} \\ &\quad - \frac{1}{2M'+1} \sum_{i=\pm(M+1)}^{\pm M'} A(i) \sin\{\omega_0[m\Delta - iD(\frac{a}{c} - \frac{a_0}{c_0})] + \phi\} \\ &= \frac{\Delta}{2\pi} \int_{-\pi}^{\pi} S(e^{j\omega m\Delta}) \left[\frac{1}{2M'+1} \sum_{i=-M'}^{M'} e^{-j\omega iD(\frac{a}{c} - \frac{a_0}{c_0})} + j\phi \frac{\omega}{\omega_0} \right. \\ &\quad \left. - \frac{1}{2M'+1} \sum_{i=\pm(M+1)}^{\pm M'} A(i) e^{-j\omega iD(\frac{a}{c} - \frac{a_0}{c_0})} + j\phi \frac{\omega}{\omega_0} \right] e^{j\omega m\Delta} d\omega \end{aligned} \quad (3.27)$$

where $S(e^{j\omega\Delta})$ is the discrete Fourier transform of $\sin\omega_m\Delta$. With ν denoting $\omega(\frac{z}{c} - \frac{z_0}{c_0})$, the magnitude of the beam pattern is

$$|W(\nu)| = \frac{1}{2M'+1} \left| \sum_{i=-M'}^{M'} e^{-jD\nu} - \sum_{i=\pm(M+1)}^{\pm M'} A(i) e^{-jD\nu} \right| \left| e^{j\phi} \frac{\omega}{\omega_0} \right|$$

$$= \frac{1}{2M'+1} \left| 1 + 2 \sum_{i=1}^{M'} \cos iD\nu - 2 \sum_{i=M+1}^{M'} A(i) \cos iD\nu \right|, \quad (3.28)$$

where the symmetry property of $A(i)$ is used. We also get a closed form for the first summation, i.e.,

$$|W(\nu)| = \frac{1}{2M'+1} \left| \frac{1 - e^{-j(2M'+1)D\nu}}{1 - e^{-jD\nu}} e^{jM'D\nu} - \sum_{i=\pm(M+1)}^{\pm M'} A(i) e^{-jD\nu} \right|$$

$$= \frac{1}{2M'+1} \left| \frac{\sin \frac{(2M'+1)D\nu}{2}}{\sin \frac{D\nu}{2}} - 2 \sum_{i=M+1}^{M'} A(i) \cos iD\nu \right|. \quad (3.29)$$

A particular case for Eqn. (3.29) is when $M'=M$ (no extrapolation), and Eqn. (3.29) degenerates to Eqn. (2.3). When $M' > M$, the beam pattern is modified by a factor $-2 \sum_{i=M+1}^{M'} A(i) \cos iD\nu$ besides the expected improvement (M being increased to M'). This is of course caused by the extrapolation error, and results in some degradation of the beam pattern.

When a window (weighting) is added in beamforming, the beam output (Eqn. (3.24)) becomes

$$\begin{aligned}
 g(a, m\Delta) = & \frac{1}{2M'+1} \sum_{i=-M'}^{M'} w(i) \sin\left[\omega_0\left(m\Delta - iD\left(\frac{a}{c} - \frac{a_0}{c_0}\right)\right) + \phi\right] \\
 & - \frac{1}{2M'+1} \sum_{i=\pm(M+1)}^{M'} w(i) A(i) \sin\left[\omega_0\left(m\Delta - iD\left(\frac{a}{c} - \frac{a_0}{c_0}\right)\right) + \phi\right] \\
 & + \frac{1}{2M'+1} \sum_{i=M'}^{M'} w(i) \tilde{H}_1\left(m\Delta - \frac{iDa}{c}\right) \quad (3.30)
 \end{aligned}$$

where the window $w(i)$ is $2M'+1$ point long, i.e., $-M' \leq i \leq M'$, and is symmetric. The corresponding beam pattern magnitude is

$$\begin{aligned}
 |W(v)| = & \frac{1}{2M'+1} \left| \sum_{i=-M'}^{M'} w(i) e^{-ijDv} - \sum_{i=\pm(M+1)}^{\pm M'} w(i) A(i) e^{-ijDv} \right| \left| e^{j\phi} \frac{w}{\omega_0} \right| \\
 = & \frac{1}{2M'+1} \left| w(0) + 2 \sum_{i=1}^{M'} w(i) \cos iDv - 2 \sum_{i=M+1}^{M'} w(i) A(i) \cos iDv \right|. \quad (3.31)
 \end{aligned}$$

Also, it degenerates to Eqn. (2.5) when $M'=M$ and degenerates to Eqn. (3.28) when $w(i)=1$ for each i , a rectangular window.

3.3.2 Signal-To-Noise Ratio

Let us reconsider Eqn. (3.25). The n_i 's are uncorrelated for each i as assumed. Also, the \hat{n}_i 's are some linear combination of n_i 's. Let h_{ij} denote the element of the $(2M'+1) \times (2M+1)$ matrix $H(HI+\gamma I)^{-1}$ at the i th row and the j th column where $-M' \leq i \leq M'$, $-M \leq j \leq M$. Thus $\hat{n}_i(m\Delta)$ can be expressed as

$$\hat{n}_i(m\Delta) = \sum_{j=-M}^M h_{ij} n_j(m\Delta); \quad M+1 \leq |i| \leq M'. \quad (3.32)$$

Then $\tilde{n}_i(m\Delta)$ can be expressed in terms of $n_i(m\Delta)$:

$$\tilde{n}_i(m\Delta) = \begin{cases} n_i(m\Delta); & |i| \leq M \\ \sum_{j=-M}^M h_{ij} n_j(m\Delta); & M+1 \leq |i| \leq M'. \end{cases} \quad (3.33)$$

Notice that the $\tilde{n}_i(m\Delta)$'s are no longer uncorrelated for $M+1 \leq |i| \leq M'$.

At the searching angle when $\frac{a}{c} = \frac{a_0}{c_0}$, Eqn. (3.24) becomes

$$\begin{aligned} g(a_0, m\Delta) = & \sin(\omega_0 m\Delta + \phi) - \frac{1}{2M'+1} \sin(\omega_0 m\Delta + \phi) \sum_{i=\pm(M+1)}^{\pm M'} A(i) \\ & + \frac{1}{2M'+1} \sum_{i=-M'}^{M'} \tilde{n}_i(m\Delta - \frac{iDa_0}{c_0}). \end{aligned} \quad (3.34)$$

The variance of $g(a_o, m\Delta)$ is ..

$$\begin{aligned}
 \text{var}[g(a_o, m\Delta)] &= \sigma_s^2 \left[1 - \frac{1}{2M'+1} \sum_{i=\pm(M+1)}^{\pm M'} A(i) \right]^2 \\
 &+ \frac{1}{(2M'+1)^2} \left[\sum_{i=-M}^M \sigma_n^2 + \sum_{i=\pm(M+1)}^{\pm M'} \sum_{j=-M}^M h_{ij}^2 \sigma_n^2 \right] \\
 &+ \frac{1}{(2M'+1)^2} \left[2 \sum_{i=\pm(M+1)}^{\pm M'} \sum_{j=-M}^M h_{ij} \sigma_n^2 \right. \\
 &\left. + \sum_{\substack{k=\pm(M+1) \\ k \neq i}}^{\pm M'} \sum_{i=\pm(M+1)}^{\pm M'} \sum_{j=-M}^M h_{kj} h_{ij} \sigma_n^2 \right] \\
 &= \sigma_s^2 \left[1 - \frac{1}{2M'+1} \sum_{i=\pm(M+1)}^{\pm M'} A(i) \right]^2 + \frac{\sigma_n^2}{(2M'+1)^2} \left[(2M+1) \right. \\
 &\left. + 2 \sum_{i=\pm(M+1)}^{\pm M'} \sum_{j=-M}^M h_{ij} + \sum_{k=\pm(M+1)}^{\pm M'} \sum_{i=\pm(M+1)}^{\pm M'} \sum_{j=-M}^M h_{kj} h_{ij} \right]
 \end{aligned}
 \tag{3.35}$$

where σ_s^2 is the variance of the signal, the same as σ_y^2 on page 11.

The signal-to-noise ratio at the beam output is then

$$\text{SNR} = 10 \log_{10} \left\{ \sigma_s^2 \left[1 - \frac{1}{2M'+1} \sum_{i=\pm(M+1)}^{\pm M'} A(i) \right]^2 \right\} - 10 \log_{10} \left\{ \frac{\sigma_n^2}{(2M'+1)^2} \left[(2M+1) \right. \right.$$

$$\begin{aligned}
& + 2 \sum_{i=\pm(M+1)}^{\pm M'} \sum_{j=-M}^M h_{ij} + \sum_{k=\pm(M+1)}^{\pm M'} \sum_{i=\pm(M+1)}^{\pm M'} \sum_{j=-M}^M h_{kj} h_{ij} \} \\
& = 10 \log_{10} \frac{\sigma_s^2}{\sigma_n^2} + 10 \log_{10} \left\{ [(2M'+1) - \sum_{i=\pm(M+1)}^{\pm M'} A(i)]^2 \right\} \\
& - 10 \log_{10} \left[(2M+1) + 2 \sum_{i=\pm(M+1)}^{\pm M'} \sum_{j=-M}^M h_{ij} + \sum_{k=\pm(M+1)}^{\pm M'} \sum_{i=\pm(M+1)}^{\pm M'} \sum_{j=-M}^M h_{kj} h_{ij} \right] \\
& = 10 \log_{10} \frac{\sigma_s^2}{\sigma_n^2} + 10 \log_{10} \left\{ [(2M'+1) - 2 \sum_{i=M+1}^{M'} A(i)]^2 \right\} \\
& - 10 \log_{10} \left[(2M+1) + 2 \sum_{i=\pm(M+1)}^{\pm M'} \sum_{j=-M}^M h_{ij} + \sum_{k=\pm(M+1)}^{\pm M'} \sum_{i=\pm(M+1)}^{\pm M'} \sum_{j=-M}^M h_{kj} h_{ij} \right]
\end{aligned} \tag{3.36}$$

where the symmetry property of $A(i)$ is again used. In the particular case when $M'=M$, all the summation terms no longer exist, and Eqn. (3.36) degenerates to

$$\begin{aligned}
\text{SNR} & = 10 \log_{10} \frac{\sigma_s^2}{\sigma_n^2} + 10 \log_{10} [(2M+1)^2] - 10 \log_{10} (2M+1) \\
& = 10 \log_{10} \frac{\sigma_s^2}{\sigma_n^2} + 10 \log_{10} (2M+1),
\end{aligned} \tag{3.37}$$

which coincides with Eqn. (2.9) for a rectangular window. For $M' > M$, we

again see from Eqn. (3.36) that besides the expected improvement, the array gain is also modified by some terms due to the extrapolation error of the signal and due to some covariances of the noise resulting from extrapolation. These modifications also degrade the SNR as in the case for beam pattern (Eqn. (3.29)). Thus, we cannot extrapolate to an infinite extent along x-axis. On the contrary, we would expect to get some optimum M' such that the quality of the overall performance would no longer increase beyond this point. It is not easy to obtain this optimum M' analytically from Eqn. (3.29) and Eqn. (3.36) since it involves the indices of the summations. However, by observing plots of digital computer simulations, it is easy to estimate the optimum M' as shown in Chapter 4.

In case a window is used in the beamformer, we should start with Eqn. (3.30). For $\frac{a}{c} = \frac{a_0}{c_0}$, we have

$$g(a_0, m\Delta) = \frac{\sin(\omega_0 m\Delta + \phi)}{2M'+1} \sum_{i=-M'}^{M'} w(i) - \frac{\sin(\omega_0 m\Delta + \phi)}{2M'+1} \sum_{i=\pm(M+1)}^{\pm M'} w(i) A(i) \\ + \frac{1}{2M'+1} \sum_{i=-M'}^{M'} w(i) \tilde{H}_i(m\Delta - \frac{iDa_0}{c_0}). \quad (3.38)$$

Its variance is

$$\text{var}[g(a_0, m\Delta)] = \frac{\sigma_s^2}{(2M'+1)^2} \left[\sum_{i=-M'}^{M'} w(i) - \sum_{i=\pm(M+1)}^{\pm M'} w(i) A(i) \right]^2$$

$$\begin{aligned}
& + \frac{\sigma_n^2}{(2M'+1)^2} \left[\sum_{i=-M}^M w^2(i) + 2 \sum_{i=\pm(M+1)}^{\pm M'} \sum_{j=-M}^M w(i) w(j) h_{1j} \right. \\
& \quad \left. + \sum_{k=\pm(M+1)}^{\pm M'} \sum_{i=\pm(M+1)}^{\pm M'} \sum_{j=-M}^M w(k) w(i) h_{kj} h_{1j} \right].
\end{aligned}
\tag{3.39}$$

Then the signal-to-noise ratio at the beam output is

$$\begin{aligned}
\text{SNR} &= 10 \log_{10} \left\{ \frac{\sigma_s^2}{(2M'+1)^2} \left[\sum_{i=-M'}^{M'} w(i) - \sum_{i=\pm(M+1)}^{\pm M'} w(i) A(i) \right]^2 \right\} \\
& - 10 \log_{10} \left\{ \frac{\sigma_n^2}{(2M'+1)^2} \left[\sum_{i=-M}^M w^2(i) + 2 \sum_{i=\pm(M+1)}^{\pm M'} \sum_{j=-M}^M w(i) w(j) h_{1j} \right. \right. \\
& \quad \left. \left. + \sum_{k=\pm(M+1)}^{\pm M'} \sum_{i=\pm(M+1)}^{\pm M'} \sum_{j=-M}^M w(k) w(i) h_{kj} h_{1j} \right] \right\} \\
&= 10 \log_{10} \frac{\sigma_s^2}{\sigma_n^2} + 10 \log_{10} \left\{ \left[\sum_{i=-M'}^{M'} w(i) - \sum_{i=\pm(M+1)}^{\pm M'} w(i) A(i) \right]^2 \right\} \\
& - 10 \log_{10} \left[\sum_{i=-M}^M w^2(i) + 2 \sum_{i=\pm(M+1)}^{\pm M'} \sum_{j=-M}^M w(i) w(j) h_{1j} \right. \\
& \quad \left. + \sum_{k=\pm(M+1)}^{\pm M'} \sum_{i=\pm(M+1)}^{\pm M'} \sum_{j=-M}^M w(k) w(i) h_{kj} h_{1j} \right].
\end{aligned}
\tag{3.40}$$

Note that this expression reduces to Eqn. (3.36) for a rectangular window and reduces to Eqn. (2.9) for $M'=M$ as expected.

CHAPTER 4

EXPERIMENTAL RESULTS

In this chapter the results of digital computer simulation will be presented. Some terminology used in the figures and in the discussion for this chapter is listed below. The observation points (number of sensors) are 17 throughout this discussion, i.e., $M=8$, as in Section 3.2. Also, the filter cutoff frequency F will be 0.05 if it is not otherwise specified.

Input SNR	signal-to-noise ratio at each sensor, dB
Beam SNR	signal-to-noise ratio at beam output, dB
xdB BW	xdB beam width of the main lobe
xdB SMER	side lobe - main lobe energy ratio when those above xdB are taken as in main lobe and those below are in side lobes, dB
SLML R	side lobe - main lobe magnitude ratio, where the largest side lobe is used, dB
Peak Loss	main lobe peak loss, dB

4.1 Main Results

Figure 4.1 shows a plot of Eqn. (3.29), beam output SNR vs. M' , the extrapolation length, for two cases when the input SNR is 30 dB and 13 dB, respectively. At the beginning point of these curves where $M'=M=8$ (no extrapolation), the beam output SNR is 42.3 dB and 25.3 dB for each

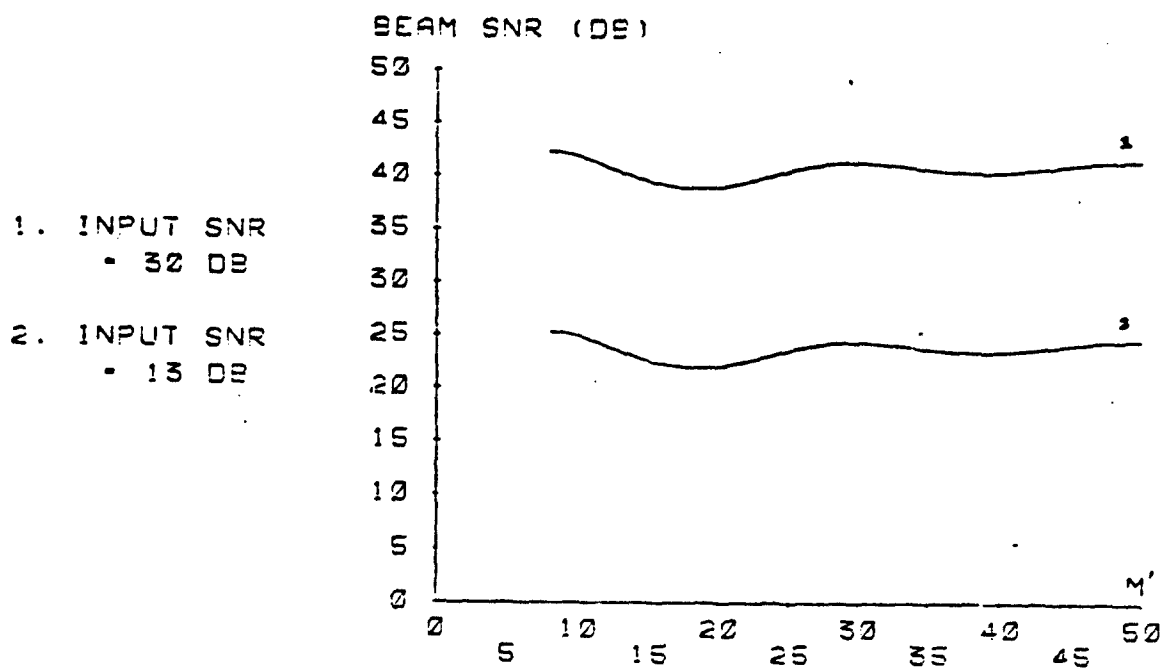


Fig. 4.1 Beam SNR vs. extrapolation length, $F=0.05$, $\gamma=0.05$

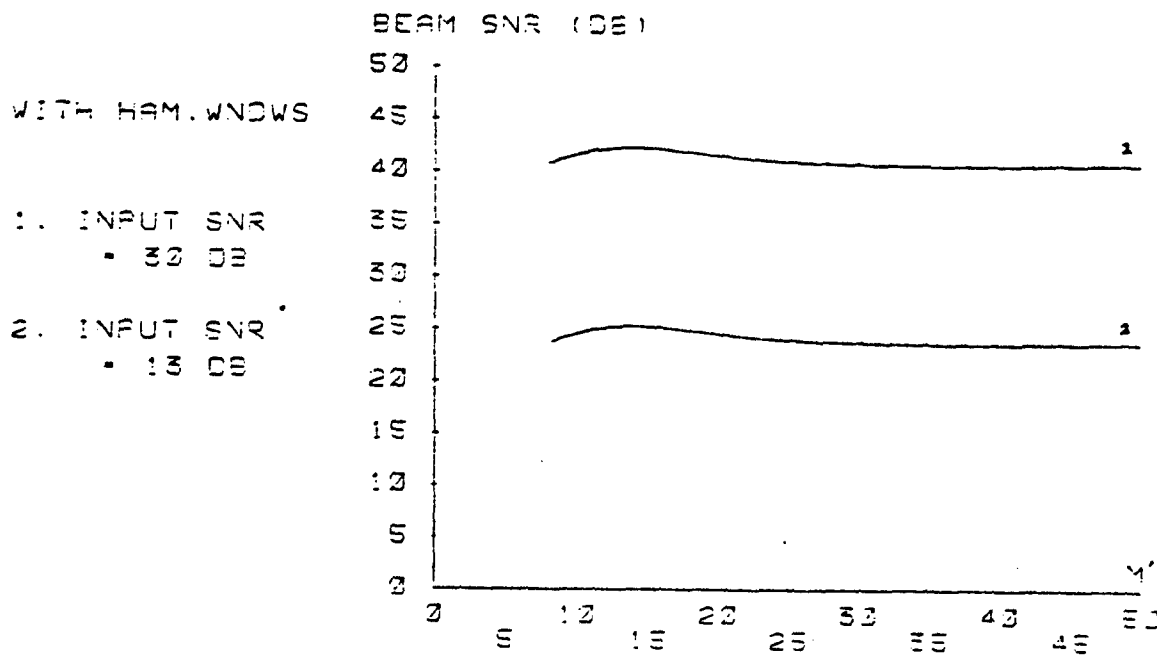


Fig. 4.2 Beam SNR vs. extrapolation length, with Hamming windows, $F=0.05$, $\gamma=0.05$

case. In other words, beamforming increases SNR by 12.3 dB. It is interesting to see that the beam SNR displays some decaying oscillation as M' increases and tends to some certain value. At $M'=29$, the beam SNR achieves a local maximum which is 41.2 dB for 30 dB input SNR and 24.3 dB for 13 dB input SNR. These values are only one dB less than those at $M'=8$. At the double length of the array, $M'=17$, the beam SNR gets the minimum value 39.0 dB and 22.0 dB, respectively. Figure 4.2 shows the same plot when Hamming windows are applied for each M' . In this case the oscillation is smoothed out. The array gain at $M'=8$ becomes 10.8 dB. The maximum value occurs at $M'=15$ where the values happen to be 42.3 dB and 25.3 dB, the same as those at $M'=8$ in Fig. 4.1. And the values at $M'=29$ equal their starting values 40.8 dB and 23.8 dB, respectively. From these plots we see that the beam SNR is not improved by extrapolation, in fact it decreases slightly. This is probably due to the strong correlation of the n_i 's and the \hat{n}_i 's.

We now observe the beam patterns. Figure 4.3 shows the beam pattern for $M'=M=8$, no extrapolation case for rectangular windows. The plots for $M'=17$ and $M'=29$ when extrapolation is applied are shown in Fig. 4.4 and Fig. 4.5. We observe that the extrapolation narrows the main lobe width extensively. Moreover, it decreases the side lobe - main lobe magnitude ratio and the side lobe - main lobe energy ratio. The peak loss is not that important since the beam SNR decreases little for these M' 's as shown in Fig. 4.1. Of course $M'=29$ is preferred since the performance of the beam pattern is slightly better than that in $M'=17$ and the degradation of SNR is only one dB. As a contrast, the beam pattern for

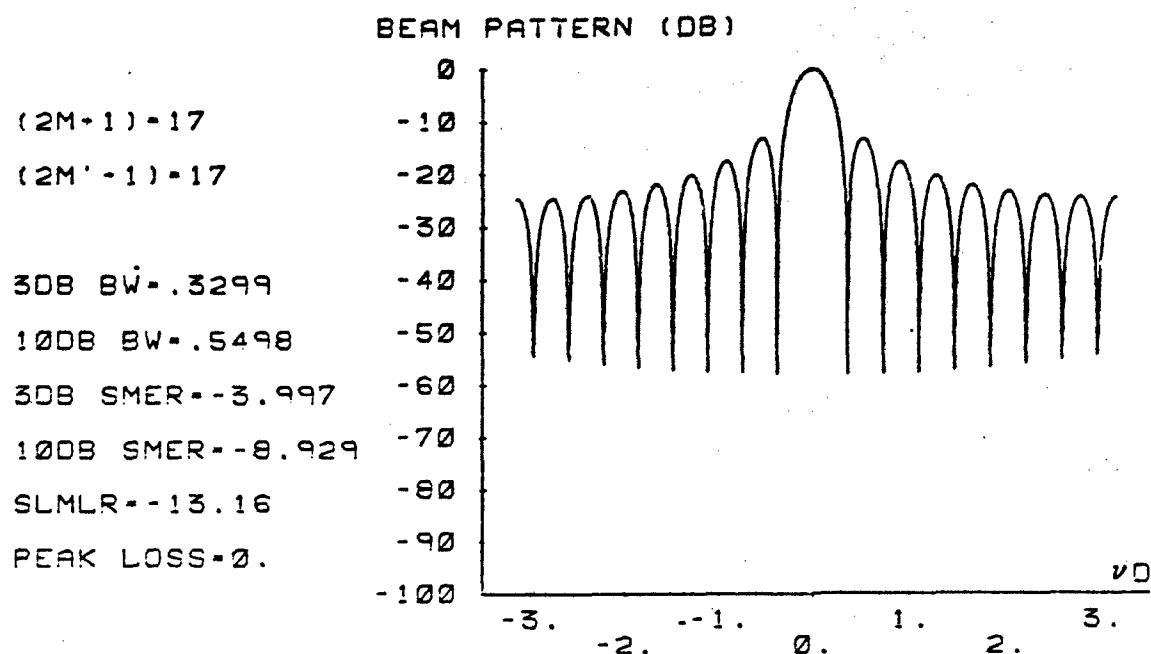
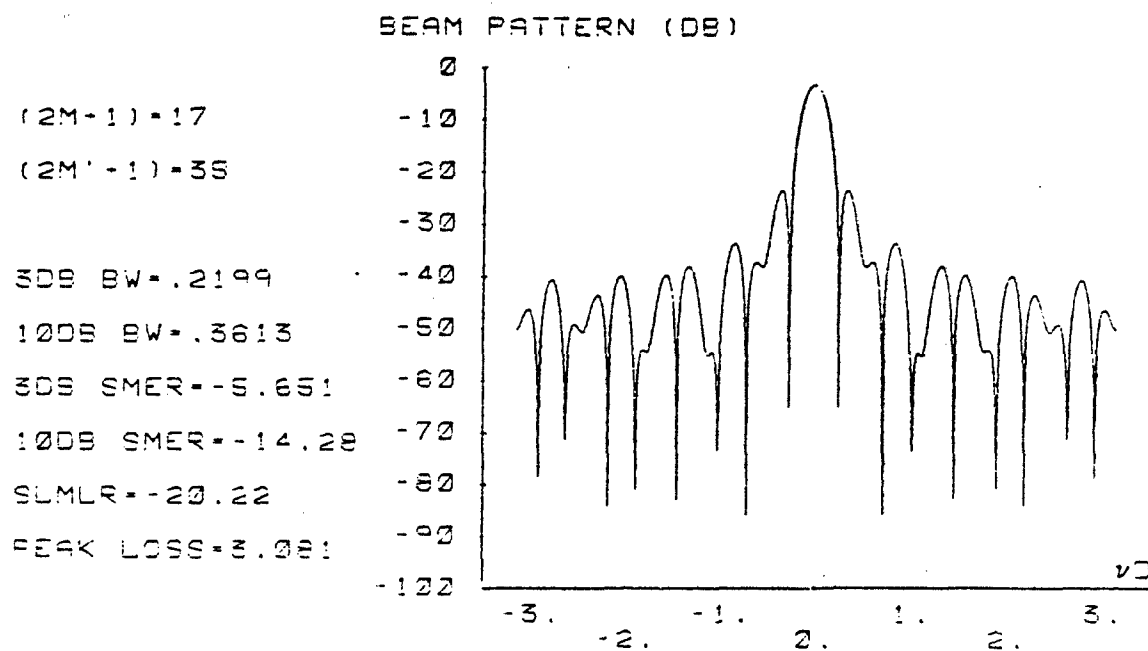


Fig. 4.3 Beam pattern for 17 sensors, no extrapolation

Fig. 4.4 Beam pattern for 17 sensors, extrapolated to 35, F=0.05, $\gamma=0.05$

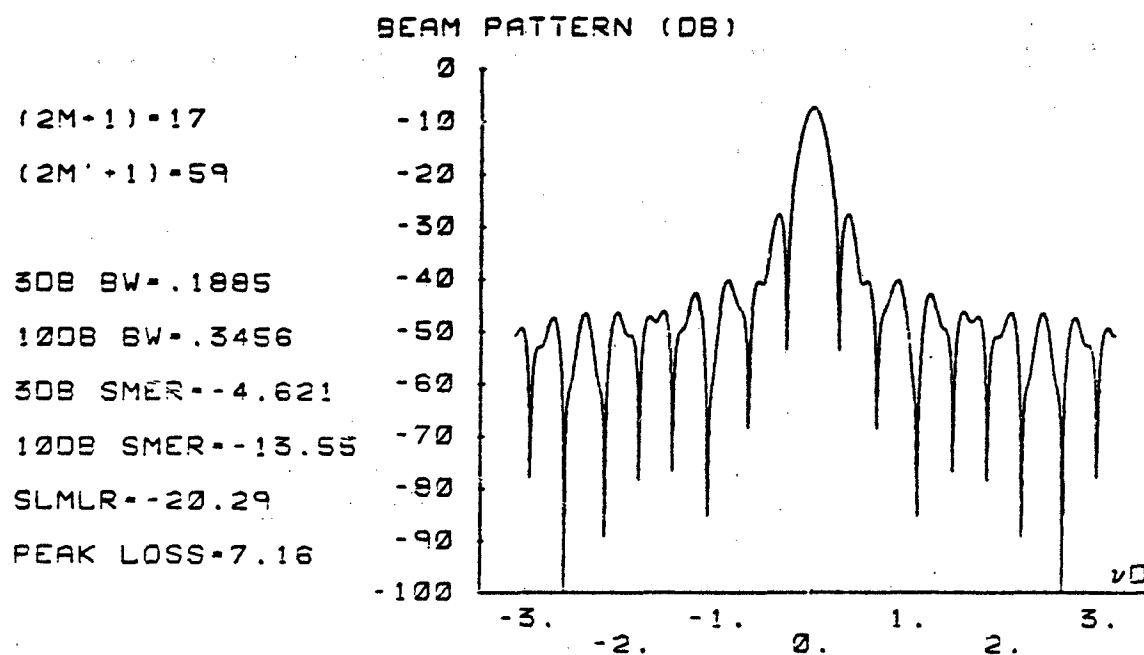


Fig. 4.5 Beam pattern for 17 sensors, extrapolated to 59, $F=0.05$, $\gamma=0.05$

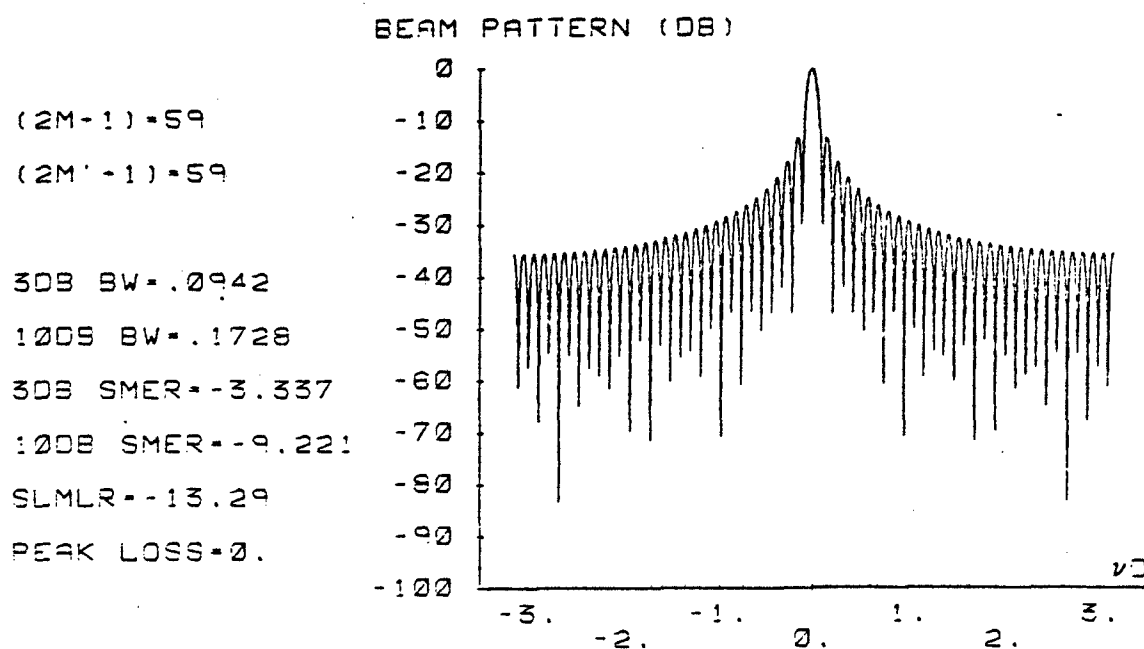


Fig. 4.6 Beam pattern for 59 sensors, no extrapolation

full observation, i.e., all the inputs to the beamformer are obtained from sensors ($M'=M$), is shown in Fig. 4.6 for $M=29$. It is seen that the beam width in this case is even narrower than that in Fig. 4.4 as we expected, since none of these 59 inputs to the beamformer contains extrapolation error. However, the side lobe - main lobe magnitude ratio and the side lobe - main lobe energy ratio remain the same. Thus, in trading off among these measurements, the digital extrapolation beamformer is compatible with a conventional digital beamformer which uses double, even triple the number of sensors. It is also observed that the improvement in the performance does not increase rapidly as M' increases. In fact beyond about $M'=40$, the side lobe - main lobe ratio starts to increase (not shown here). Thus, in consideration of complexity of implementation and the improvement of the performance, $M'=29$ is approximately optimum in this case.

When Hamming windows are applied in the digital extrapolation beamformer, results are obtained as shown in Fig. 4.7 through Fig. 4.10. Figure 4.7 shows the case when no extrapolation is applied to the 17 sensors. Comparing it with Fig. 4.3, it is clear that the application of Hamming windows decreases the side lobe - main lobe ratio on the expense of widening the main lobe. The results of applying extrapolation are still good as shown in Fig. 4.8 and Fig. 4.9. The main lobe is narrowed while the side lobe - main lobe magnitude ratio is further reduced than the cases without applying Hamming windows. The extrapolation length $M'=15$ is preferred because of its smallest side lobe - main lobe magnitude ratio (-27 dB) and largest beam SNR (see Fig. 4.2). For $M'=29$

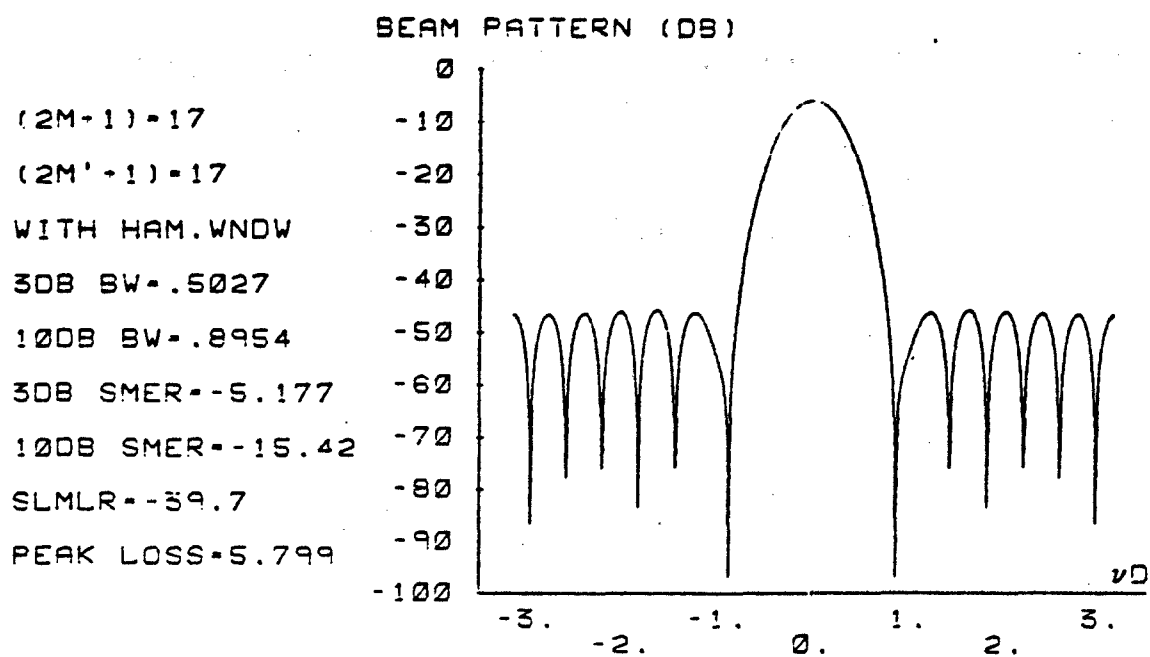


Fig. 4.7 Beam pattern for 17 sensors with a Hamming window, no extrapolation

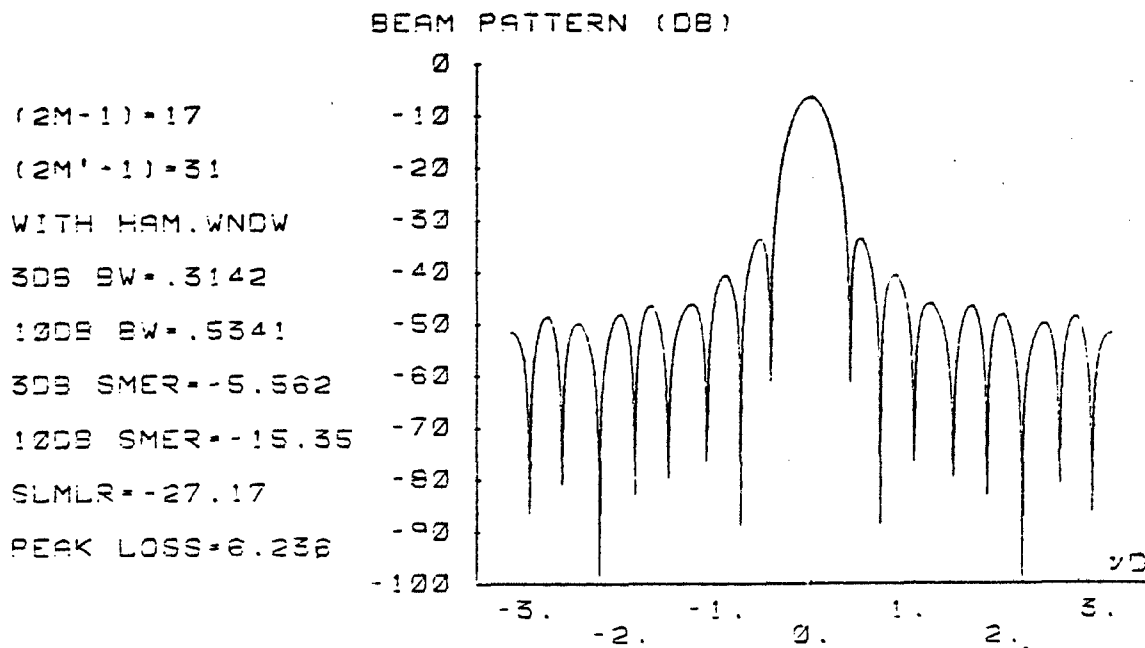


Fig. 4.8 Beam pattern for 17 sensors, extrapolated to 31, with a Hamming window, $F=0.05$, $\gamma=0.05$

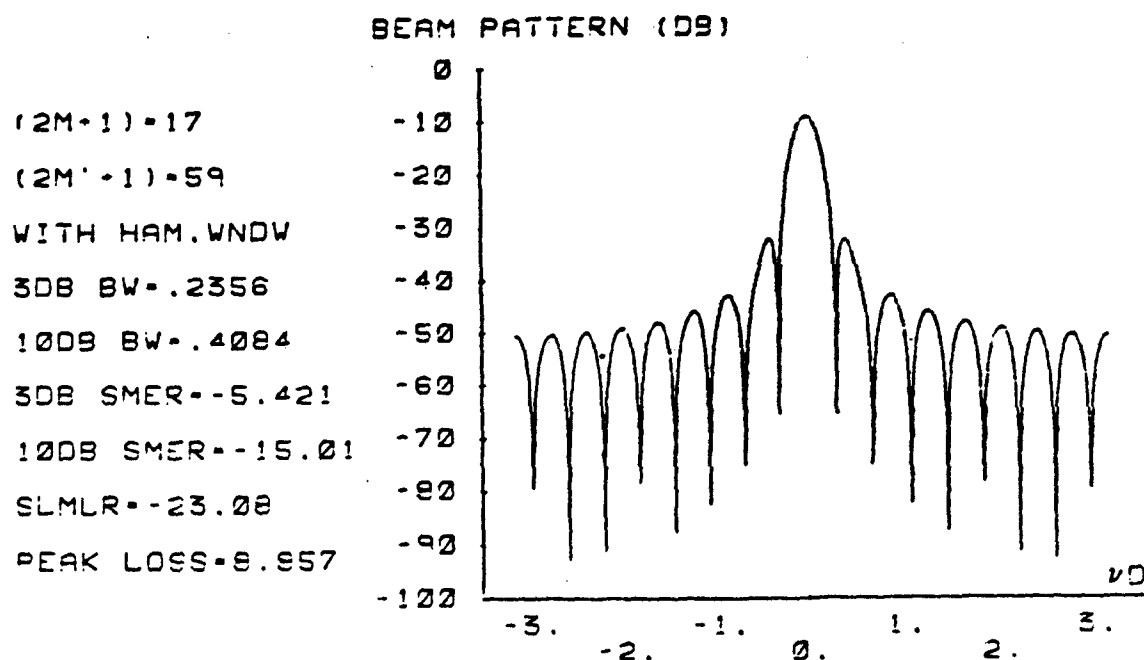


Fig. 4.9 Beam pattern for 17 sensors, extrapolated to 59, with a Hamming window, $F=0.05$, $\gamma=0.05$

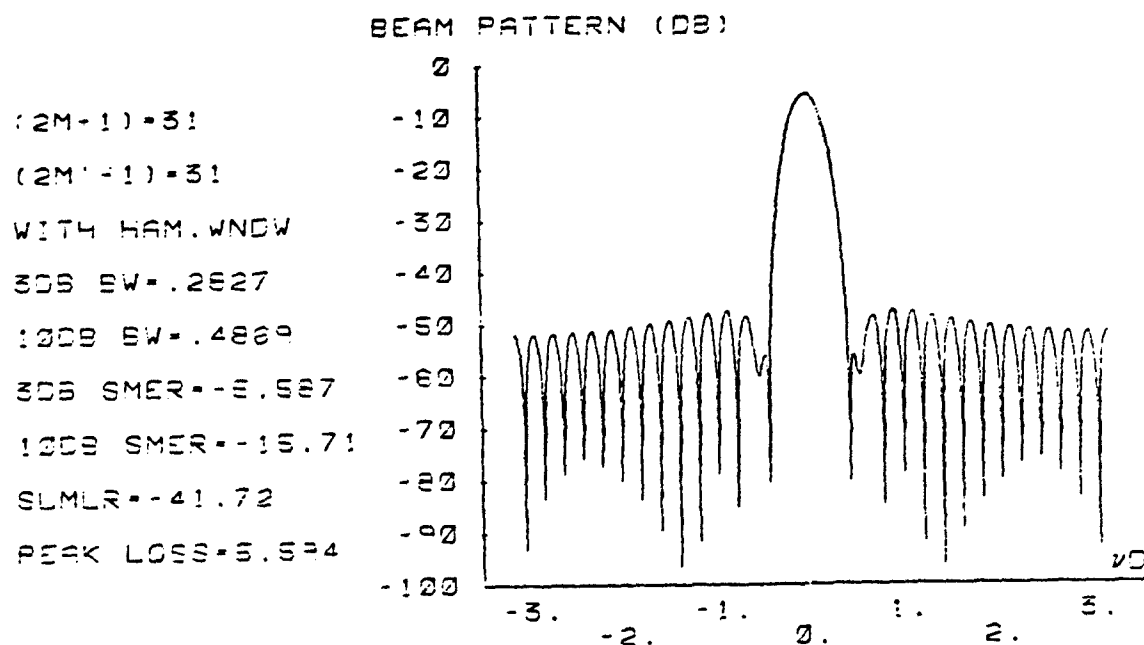


Fig. 4.10 Beam pattern for 31 sensors with a Hamming window, no extrapolation

(Fig. 4.9), the side lobe - main lobe magnitude ratio is only -23 dB, thus we would have used the case shown in Fig. 4.5 where much narrower main lobe overwhelms the compatible side lobe - main lobe magnitude ratio with the former. Figure 4.10 serves again as a contrast which is obtained using full observation of 31 sensors. We see that the side lobe reduction for the extrapolation beamformer is not as good as that for the conventional beamformer in applying Hamming windows.

4.2 Effects Of Parameter Changes

As we mentioned earlier, the parameters F and γ can be changed to alter the performance. To gain more insight into this, we now observe the case when $F=0.1$. Figure 4.11 and Fig. 4.12 show the beam SNR for rectangular windows and Hamming windows as before. They show same character as that in Fig. 4.1 and Fig. 4.2 except that the oscillation frequency is increased in Fig. 4.11. Two peaks nearest to the origin along M' -axis are at $M'=19$ and $M'=29$. The beam patterns at these points are shown in Fig. 4.13 and Fig. 4.14 (The beam pattern for $M'=M=8$ is same as that in Fig. 4.3 since no extrapolation is involved when $M'=M$). We see that all measurements are not as good as that shown in Fig. 4.4 and Fig. 4.5 while they are still much better than those in Fig. 4.3. The case when Hamming windows are applied is shown in Fig. 4.15 and Fig. 4.16 for $M'=13$ (where beam SNR gets the largest value) and $M'=19$ (in contrast with Fig. 4.13). The same observation is made as the case with the rectangular windows. It is also observed for both cases that the improvement in the beam pattern increases more slowly as M' increases.

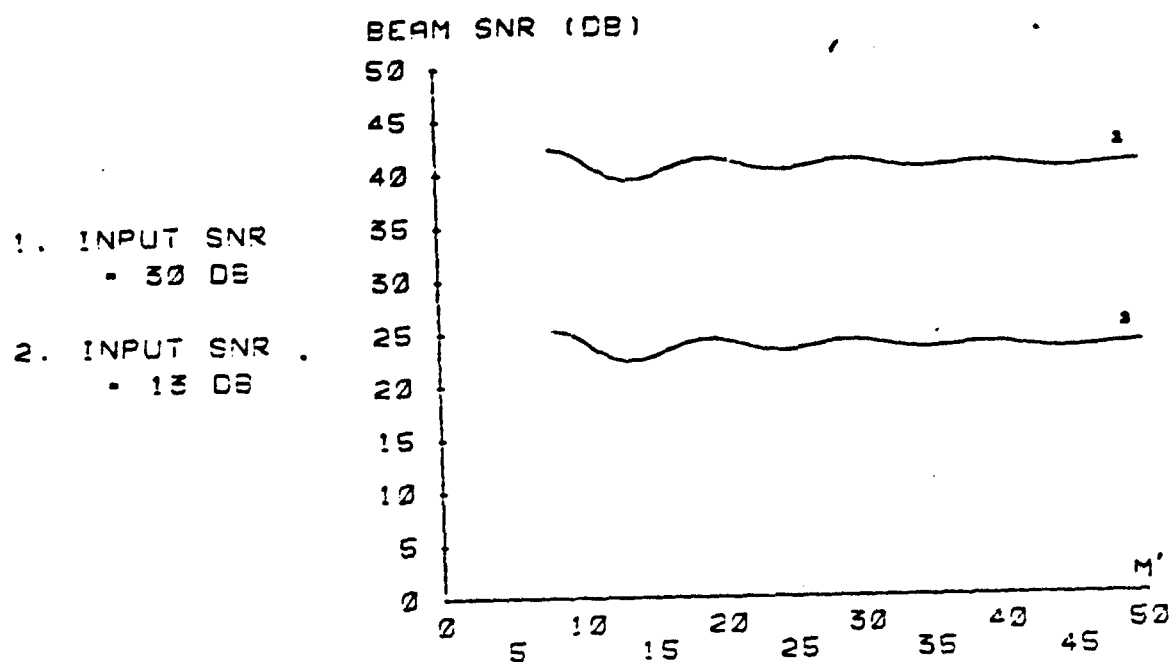


Fig. 4.11 Beam SNR vs. extrapolation length, $F=0.1$, $\gamma=0.05$

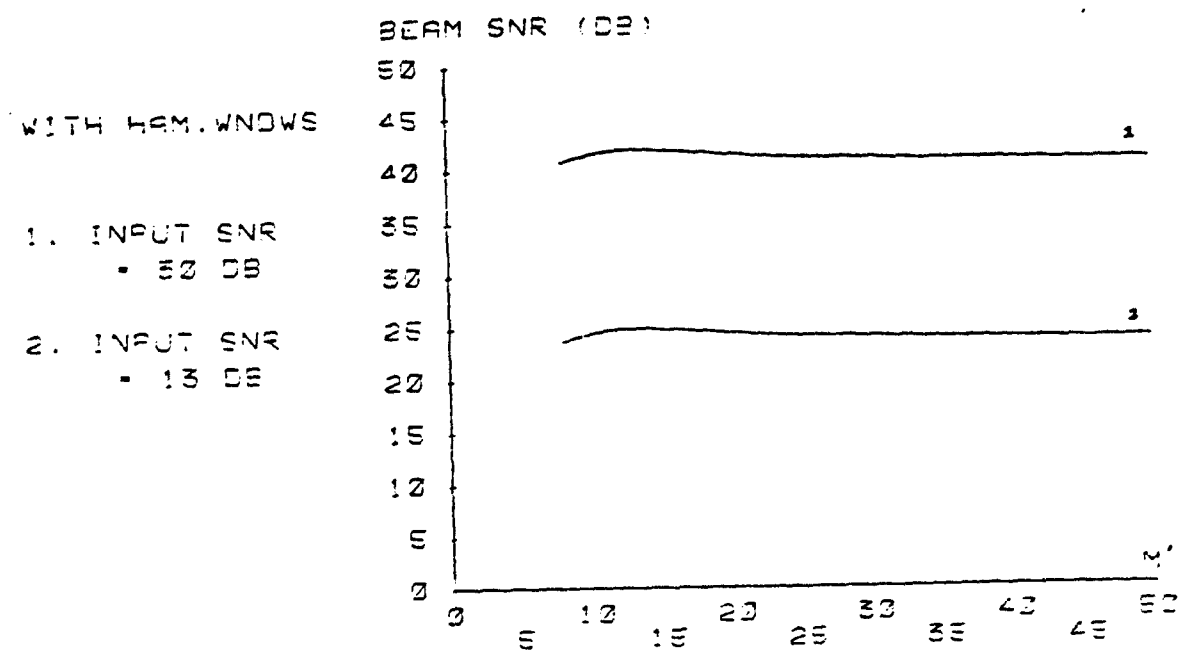


Fig. 4.12 Beam SNR vs. extrapolation length,
with Hamming windows, $F=0.1$, $\gamma=0.05$

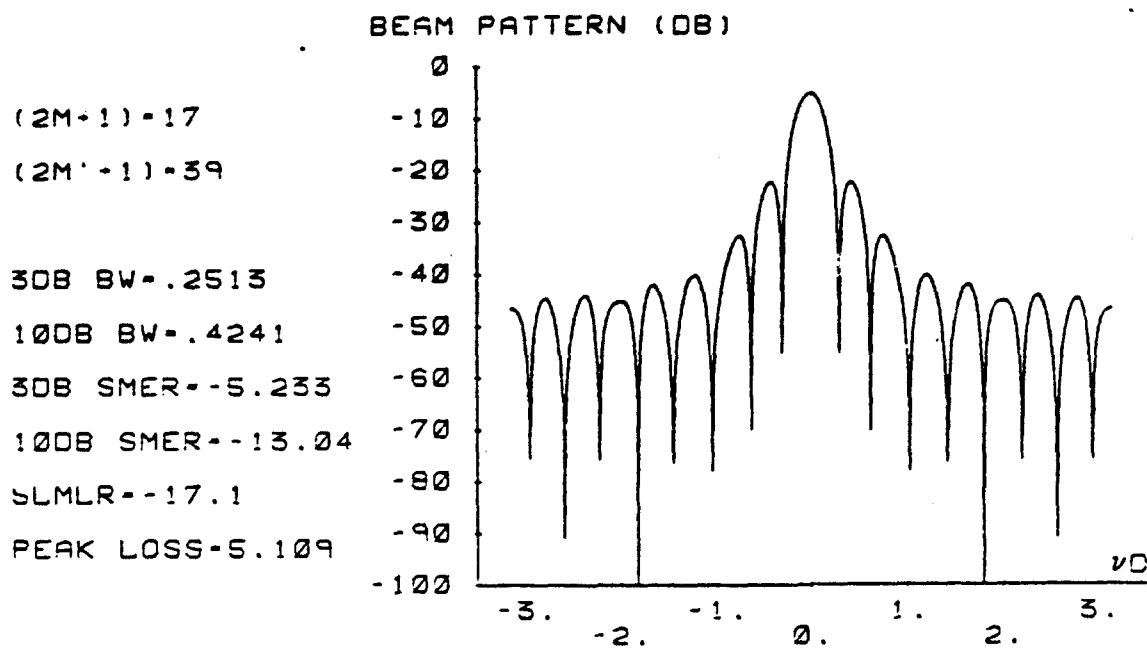


Fig. 4.13 Beam pattern for 17 sensors, extrapolated to 39, $F=0.1$, $\gamma=0.05$

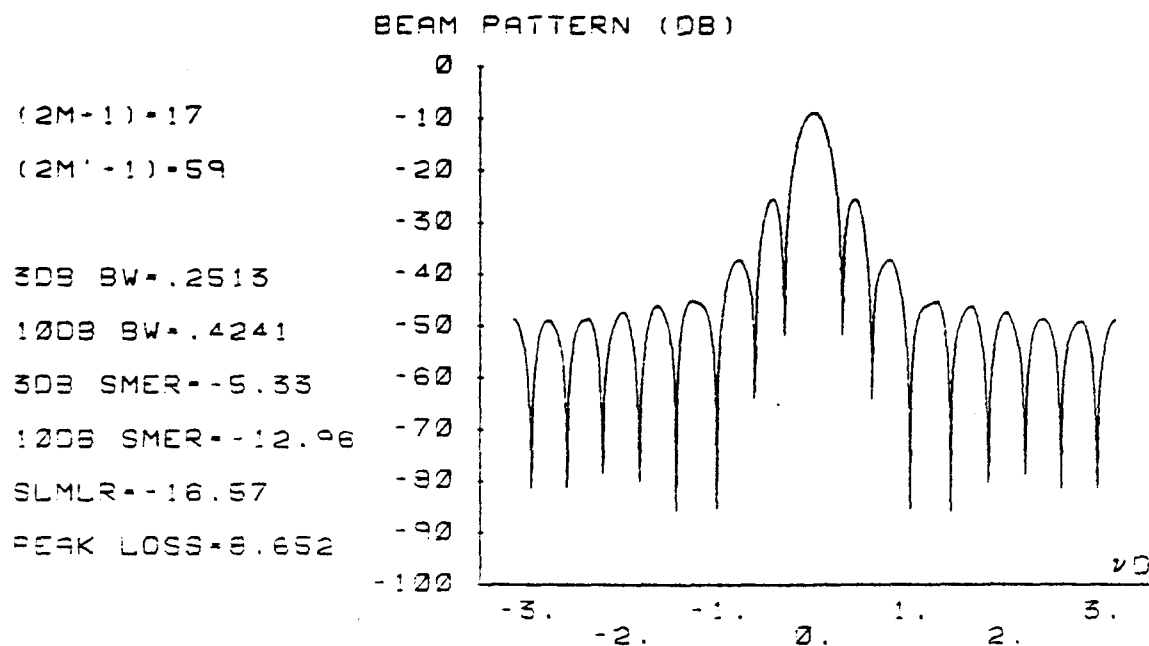


Fig. 4.14 Beam pattern for 17 sensors, extrapolated to 59, $F=0.1$, $\gamma=0.05$

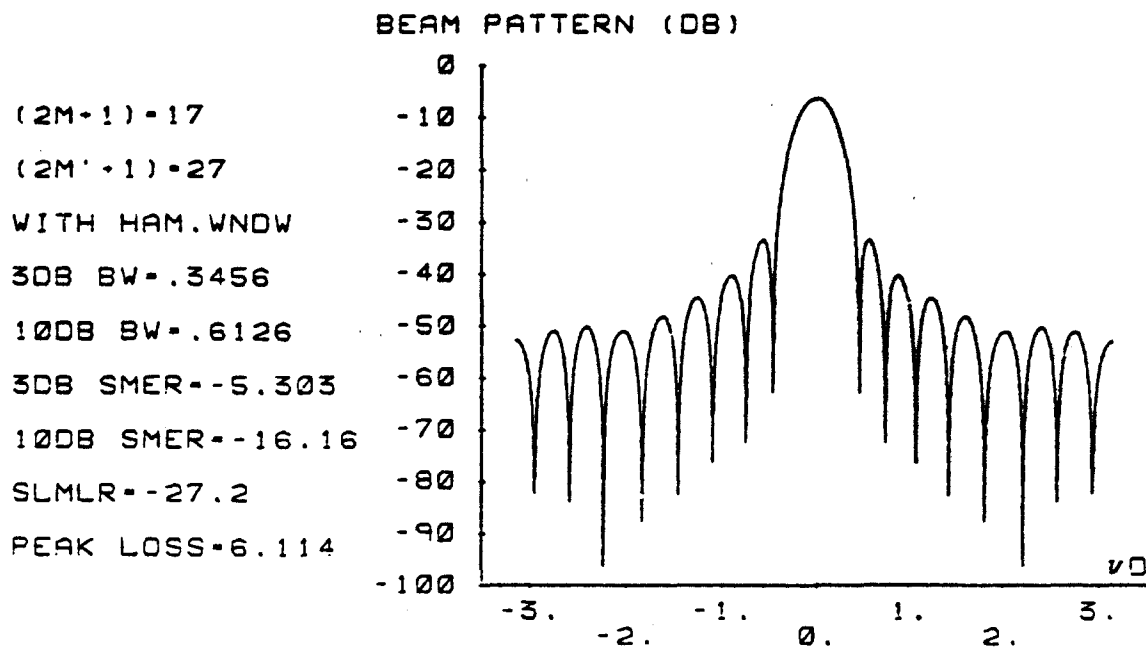


Fig. 4.15 Beam pattern for 17 sensors, extrapolated to 27, with a Hamming window, $F=0.1$, $\gamma=0.05$

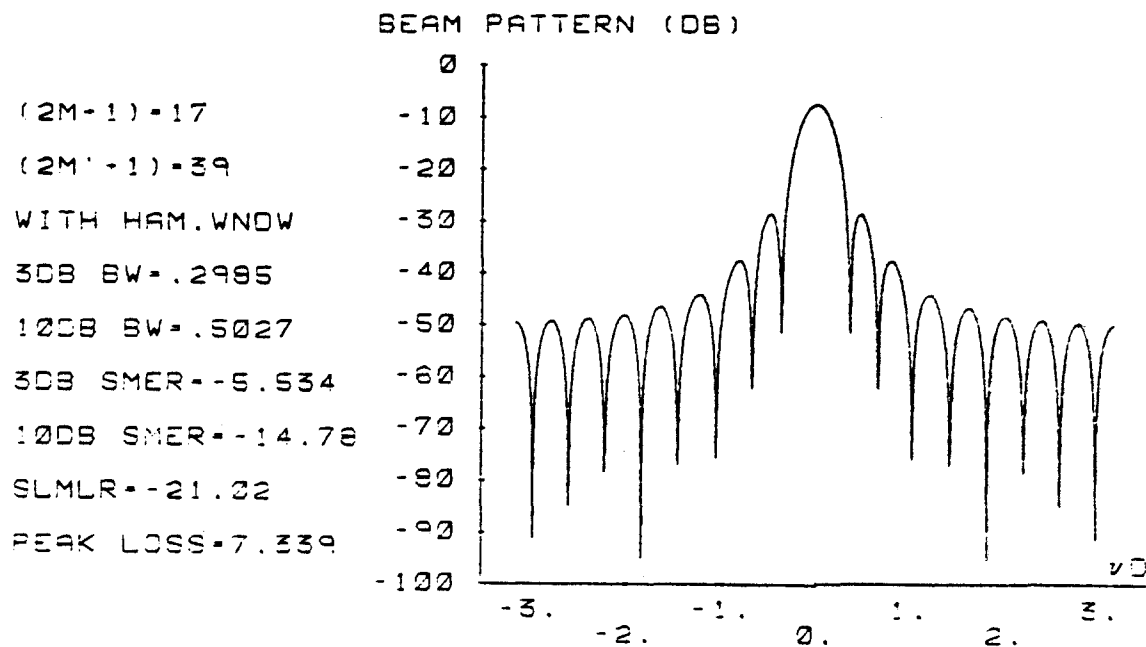


Fig. 4.16 Beam pattern for 17 sensors, extrapolated to 39, with a Hamming window, $F=0.1$, $\gamma=0.05$

We conclude from these observations that smaller extrapolation filter frequency F performs better. This coincides with the criterion (2) (Observation (2)) in Section 3.2. Thus it is important to select D and f_c ($F=f_c \frac{D}{c_0}$) such that Eqn. (3.5), Eqn. (3.19) and the criterion (2) in Section 3.2 are met in designing a digital extrapolation beamformer.

All the experiments shown above were conducted under the assumption that the parameter γ in Eqn. (2.17) is chosen such that $10\log_{10} \frac{1}{\gamma}$ is 13 dB even if the input SNR ($=10\log_{10} \frac{\sigma_s^2}{\sigma_n^2}$) is not 13 dB. This is because, for one reason, the hardware implementation (see Fig. 3.2) requires that γ be fixed. Besides, the input SNR is usually not known in a practical situation, this also requires a good guess for γ . The value for γ that has been used can then be changed. A group of plots is shown in Fig. 4.17 through Fig. 4.20 for beam SNR and beam pattern as we did before, where γ is chosen such that $10\log_{10} \frac{1}{\gamma}$ is 30 dB. We observe the similar behavior with the previous ones while some differences are also noticed. The beam SNR performs worse in the sense that it tends to some lower value (even lower than input SNR) and decreases very fast as M' departs from 8. On the other hand, however, the beam pattern performs better in the sense that the main lobe width is narrower and the side lobe - main lobe ratio is smaller compared with the previous corresponding ones. This gives us another degree of freedom in choosing parameters to compensate among various design requirement and various measurements of performance.

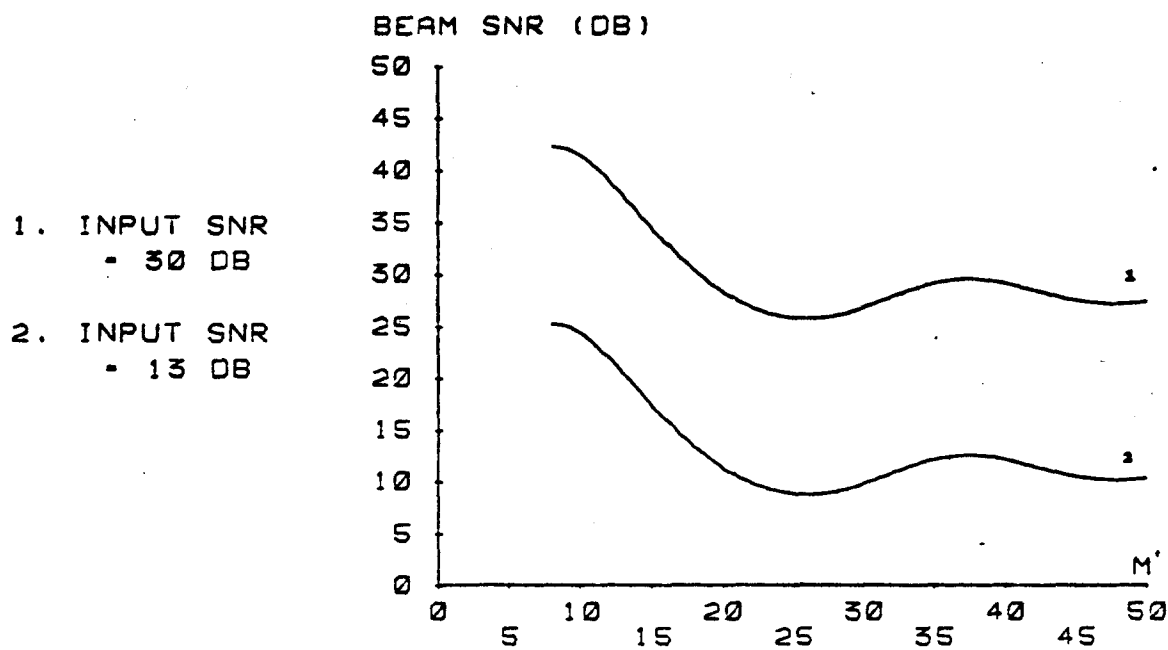


Fig. 4.17 Beam SNR vs. extrapolation length, $F=0.05$, $\gamma=0.001$

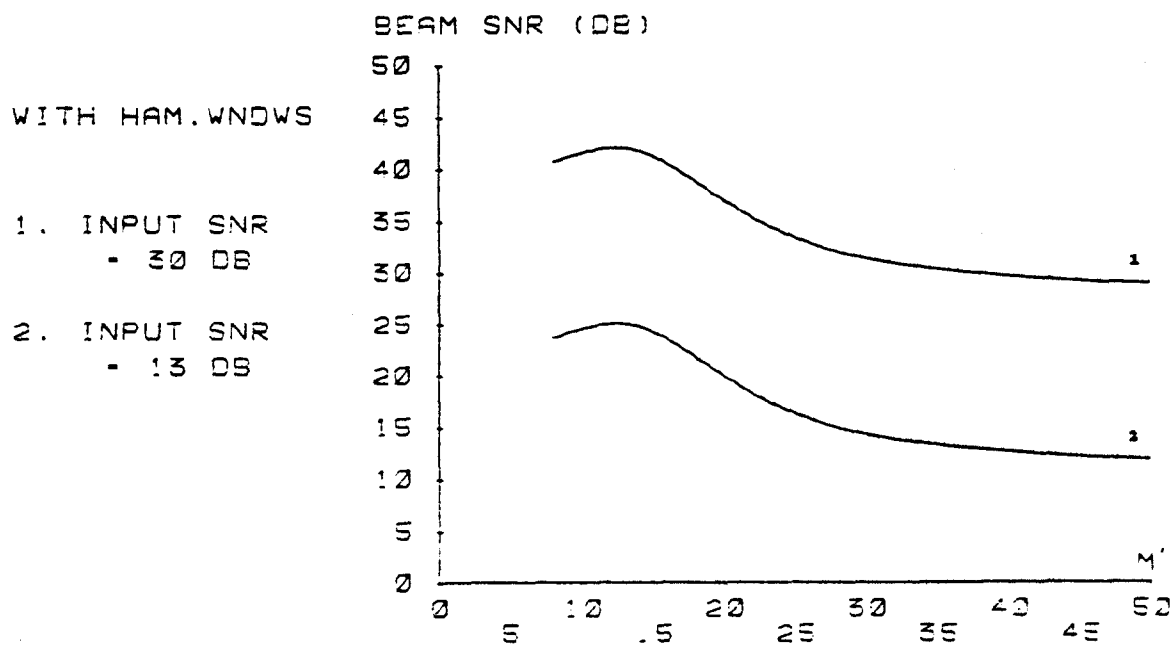


Fig. 4.18 Beam SNR vs. extrapolation length, with Hamming windows, $F=0.05$, $\gamma=0.001$

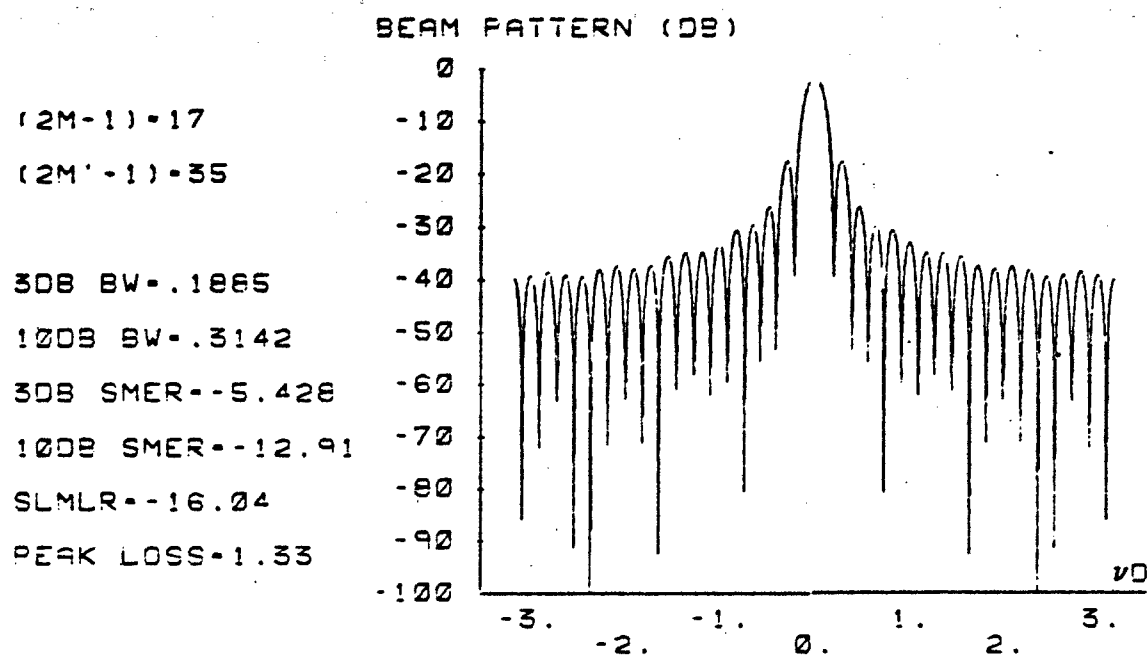


Fig. 4.19 Beam pattern for 17 sensors, extrapolated to 35, $F=0.05$, $\gamma=0.001$

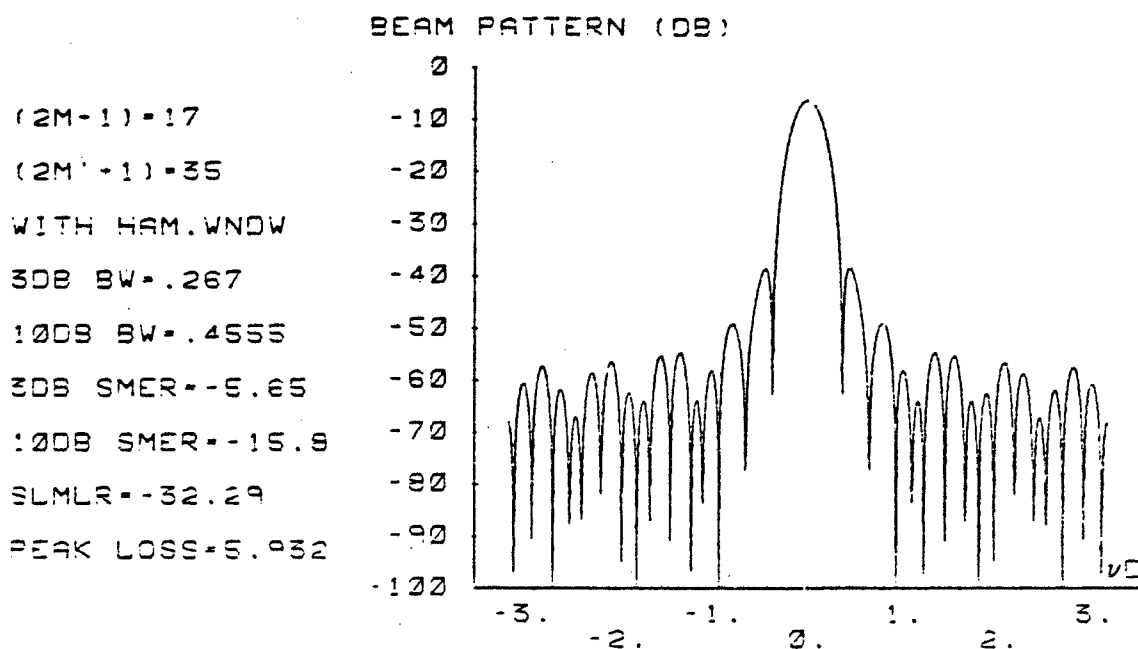


Fig. 4.20 Beam pattern for 17 sensors, extrapolated to 35, with a Hamming window, $F=0.05$, $\gamma=0.001$

CHAPTER 5

SUMMARY

In this thesis the application of spatial extrapolation in digital beamforming was studied. An essential problem in evaluating performance of the digital extrapolation beamformer is to model the extrapolation error. Section 3.2 was devoted to this issue for both finite energy signals and periodic signals. An error model was obtained as a random function with certain distribution for a particularly important kind of signals, sinusoidal input signals. Having accomplished this, it is not difficult to construct a real-time hardware implementation scheme.

A large amount of digital computer simulation was done for various cases. The results are quite promising. It was shown that the beam pattern can in general be improved extensively, in some cases we can even extrapolate as far as the double length or triple length of the physical sensors with the performance compatible to a conventional digital beamformer with this large amount of sensors. On the other hand, however, signal-to-noise ratio is degraded slightly by the extrapolation. A parameter γ can be chosen to compensate between these two measurements.

Other techniques such as windowing, temporal interpolation, etc. can be combined with the spatial extrapolation to improve performance further. Examples using Hamming windows were included.

Since the sinusoidal wave is a basis function for other signals through Fourier series and Fourier integral, and the one-step extrapolation process is linear, the results obtained in this thesis can

be readily extended to the general case. On the other hand, however, sinusoidal wave contains infinite energy. The convergence of its discrete extrapolation to its continuous value has not been proven yet [13]. This, together with a theoretical model for its extrapolation error, remains open questions in the digital extrapolation beamforming.

REFERENCES

- [1] D. E. Dudgeon, "Fundamentals of Digital Array Processing," Proceedings of IEEE, Vol. 65, No. 6, pp. 898-904, June, 1977.
- [2] R. G. Pridham and R. A. Mucci, "Digital Interpolation Beamforming for Low-Pass and Bandpass Signals," Proceedings of IEEE, Vol. 67, No. 6, pp. 904-919, June 1979.
- [3] P. Rudnick, "Digital Beamforming in the Frequency Domain," Journal of Acoustical Society of America, Vol. 46, No. 5, pp. 1089-1090, 1969.
- [4] G. L. De Muth, "Frequency Beamforming Techniques," in 1977 IEEE International Conference on Acoustics, Speech and Signal Processing (Hartford, CT), pp. 713-715, 1977.
- [5] S. P. Pitt, W. T. Adams, and J. K. Vaughan, "Design and Implementation of a Digital Phase Shift Beamformer," Journal of Acoustical Society of America, Vol. 64, No. 3, pp. 808-814, September 1978.
- [6] R. G. Pridham and R. A. Mucci, "A Novel Approach to Digital Beamforming," Journal of Acoustical Society of America, Vol. 63, No. 2, pp. 425-434, February, 1978.
- [7] R. G. Pridham and R. A. Mucci, "Shifted Sideband Beamformer," IEEE Transactions on Acoustics, Speech and Signal Processing, Vol. ASSP-27, No. 6, pp. 713-722, December 1979.
- [8] W. C. Knight, R. G. Pridham, and S. M. Kay, "Digital Signal Processing for Sonar," Proceedings of IEEE, Vol. 69, No. 11, pp. 1451-1506, November 1981.
- [9] A. Papoulis, "A New Algorithm in Spectral Analysis and Band-Limited Extrapolation," IEEE Transactions on Circuits and Systems, Vol. CAS-22, No. 9, pp. 735-742, September 1975.
- [10] J. A. Cadzow, "An Extrapolation Procedure for Band-Limited Signals," IEEE Transactions on Acoustics, Speech and Signal Processing, Vol. ASSP-27, No. 1, pp. 4-12, February 1979.

- [11] A. Sonnenschein and B. W. Dickinson, "On a Recent Extrapolation Procedure for Band-Limited Signals," IEEE Transactions on Circuits and Systems, Vol. CAS-29, No. 2, pp. 116-117, February 1982.
- [12] A. K. Jain and S. Ranganath, "Extrapolation Algorithms for Discrete Signals with Application in Spectral Estimation," IEEE Transactions on Acoustics, Speech and Signal Processing, Vol. ASSP-29, No. 4, pp. 830-845, August 1981.
- [13] J. L. C. Sanz and T. S. Huang, "Discrete and Continuous Band-Limited Signal Extrapolation," to be published.
- [14] J. H. McClellan and T. W. Parks, "A Unified Approach to the Design of Optimum FIR Linear Phase Digital Filters," IEEE Transactions on Circuit Theory, Vol. CT-20, pp. 697-701, November 1973.
- [15] A. V. Oppenheim and R. W. Schaffer, Digital Signal Processing, Englewood Cliffs, New Jersey: Prentice-Hall, Chap. 5, 1975.
- [16] A. V. Tikhonov and V. Y. Arsenin, Solutions of Ill-Posed Problems, Washington, D. C.: V. H. Winston Sons, pp. 1-4, 1977.
- [17] L. J. Cutrona, "Comparison of Sonar System Performance Achievable Using Synthetic-Aperture Techniques with the Performance Achievable by More Conventional Means," Journal of Acoustical Society of America, Vol. 58, No. 2, pp. 336-348, August 1975.